AWARD NO. 01HQGR0059

FINAL TECHNICAL REPORT

November 2, 2004

MAPS OF GROUND MOTION AMPLIFICATION REPRESENTING THE 3D EFFECTS OF THE MISSISSIPPI EMBAYMENT ON WAVE PROPAGATION

Principal Investigator: Chandan K. Saikia
Co-Investigators: Arben Pitarka and Gene A. Ichinose
URS Group, Inc.

566 El Dorado Street - 2nd Floor
Pasadena CA 91101-2560
Tel: (626)-449-7650
Fax: (626)-449-3536

email: chandan_saikia@urscorp.com

Program Element: I. Products for Earthquake Loss Reduction

AWARD NO. 01HQGR0059

FINAL TECHNICAL REPORT

November 2, 2004

MAPS OF GROUND MOTION AMPLIFICATION REPRESENTING THE 3D EFFECTS OF THE MISSISSIPPI EMBAYMENT ON WAVE PROPAGATION

Principal Investigator: Chandan K. Saikia
Co-Investigators: Arben Pitarka and Gene A. Ichinose
URS Group, Inc., Pasadena, CA 91101

566 El Dorado Street, Pasadena, CA 91101
Tel: (626)-449-7650
Fax: (626)-449-3536

email: chandan_saikia@urscorp.com
Program Element: I. Products for Earthquake Loss Reduction

Non-Technical Abstract

In this study we attempt to constrain ground motion characteristics within and around the Mississippi embayment and evaluate effects of the embayment structure on wave propagation by analyzing both two- and three-dimensional responses of the irregular basement structure of the Mississippi embayment. To accomplish our goals, we collected waveform data from both strong- and weak-motion networks operating in the Mississippi Embayment to identify the salient features of the embayment structure. We analyzed waveforms from earthquakes in the Mississippi Embayment and determine how well the waveforms can be modeled using only the 1D models or whether the waveforms would require station specific crustal models. We used waveforms from previously investigated earthquakes by other investigators, utilized the established focal mechanisms and depths therein, and refined the initial 1D model as needed. We have also examined the effect of irregular crustal model by simulating finite-difference seismograms using two-dimensional crustal models extending from the City of Saint Louis in Missouri to Memphis in Arkansas (Catchings, 1999). The source was embedded at two separate locations and finite-difference

seismograms were used to distinguish features in the seismic wave propagation from the Mississippi Embayment towards the Illinois basin and vice versa. We have also collected geologic information of the Mississippi Embayment region, which incorporates material properties of the shallow structure in order to establish a working three-dimensional model of the study region. Based on the three-dimensional finite-difference seismograms (up to 2 seconds) simulated for a large scenario earthquake in the New Madrid seismic zone we expect the deep structure of the Mississippi Embayment to have little impact on the ground motion amplitudes for periods of two seconds and shorter. We estimated the amplification at these periods by calculating the transfer function relative to a 1D model of the Mississippi Embayment (Table 3), the upper four layers representing the sedimentary rocks of the Mississippi Embayment. By smoothing the amplification function of the 1D model, the long period amplification function (i.e., the ratio of the 3D Mississippi Embayment to 1D hard rock simulations) appears primarily caused by the impedance contrast and is larger than the deamplification, which is due to rock damping effects, thus the net amplification is equivalent to an 1D effect of the impedance contrast at the basement. However, for periods < 0.1s, the amplification due to impedance contrast is smaller than the deamplification caused by the rock damping effects, thus a net deamplification.

Introduction

In this study we attempt to constrain ground motion characteristics within and around the Mississippi embayment and evaluate effects of the embayment structure on wave propagation by analyzing both two- and three-dimensional responses of the irregular basement structure of the Mississippi embayment. To accomplish our goals, we collected waveform data from both strong- and weak-motion networks operating in the Mississippi Embayment to identify the salient features of the embayment structure. There are three strong-motion networks, which are operated by LDEO (Lamont Doherty Earth Observatory), USGS and University of Kentucky (Figure 1) in addition to the broadband stations that are operated by CERI (Center of Earthquake Research Institute, Memphis). In this investigation, we analyze waveforms from earthquakes in the Mississippi Embayment and determine how well the waveforms can be modeled using only 1D models or whether the waveforms would require station specific crustal models. In this regard, we utilize earthquakes that were

previously studied by other investigators (Langston, 1994), utilize focal mechanisms and depths therein, and refine the initial 1D model as needed. We use the technique discussed in Xu and Wein (1997) in which the misfit in waveforms of individual stations is minimized to delineate variations in the respective crustal models. In the following sections, we discuss overall characteristics of strong-motion data, modeling of 2001 Enola Arkansas, 1991 Risco and 1990 Cape Girardeau earthquakes (Table 1) to probe suitability of 1D models of the Mississippi Embayment and examine the basin effects on the amplitude and duration of the waveforms recorded at a wide range of distances.

In addition, we have also examined the effect of irregular crustal model by simulating finite-difference seismograms using two-dimensional crustal models extending from Memphis in Tennessee to the City of Saint Louis in Missouri (Catchings, 1999). The source was embedded at two separate locations and simulated seismograms were used to examine features that distinguish the seismic wave propagation from the Mississippi Embayment towards the Illinois basin and vice versa. We have also collected geologic information of the Mississippi Embayment region, which incorporates material properties of the shallow structure in order to establish a working three-dimensional model of the study region.

Strong-Motion and Long Period Broadband Data as Recorded in the Mississippi Embayment

Figure 1 displays the distribution of strong-motions that operated in the Mississippi Embayment. These stations have recorded earthquakes (green circles, right panel Figure 1), which occurred within and around the embayment structure. Figure 2 shows strong-motion and the corresponding velocity waveforms recorded by three stations, namely RIDGE, RSCO and LOAP, from the Cape Girardeau earthquake in Missouri (09/26/90, mb=4.7, 37.2319^{o}N and 89.6429^{o}W, depth=12km). In an earlier study, Langston (1994) has modeled its regional seismograms in great detail. Figure 3 shows a map of SLU (Saint Louis University), USNSN and IU broadband stations in New Madrid that recorded the 1990 Cape Girardeau, Missouri, 1991 Risco, Missouri and 2001 Enola, Arkansas earthquakes. In this study, we have performed a detailed analysis of regional waveforms recorded from the Enola earthquake.

We collected available regional and far-regional waveforms from the IRIS data center and used the long-period (5-50s) waves recorded at 11 stations at distances extending from 320 km to 1300 km in this effort. Figure 4 shows synthetic waveforms and their agreement with the observed data. We inverted long-period data to determine moment-tensor solution and depth, and determined that the fault associated with this earthquake dips steeply at an angle of 85°. Clearly many of the stations are nodal as indicated by the strong transverse ground motions. For paths crossing the embayment we required a low velocity layer at the top of the model and paths to stations CCM and SLM crossing the Ozark Mountain did not need low velocity zone. Next, we have used the regional seismograms recorded at station CCM from these earthquakes to investigate whether any further analysis will permit us to constrain the thickness of the near-surface sedimentary structure underneath this station.

Estimation of Station-Specific 1D Crustal Structure - Method

Following Xu and Wein (1997), we use difference seismograms constructed using data and synthetic seismograms to form the data vector (Δd) and expressed it as a linear combination of the first-order partial derivatives (DG) times the first-order velocity perturbation (Δm) as follows

$$\Delta d = \mathbf{DG}.\Delta m$$

To employ this approach, we discretize the initial velocity model and construct synthetic seismograms, $\mathbf{S_o(t)}$, using source parameters consisting of focal parameters (dip, slip and strike of the fault), source depth and seismic moment **(Mo)** previously determined by modeling of the long-period recorded seismograms. Since we are interested in finding the effects of the near-surface crustal layers representing the sediment structure of the Mississippi embayment, we finely discretize the upper crust (say the upper 4-6 km of the crust) and leave the remaining of the velocity model unchanged. The vector **DG** is a matrix consisting of partial derivatives, where the $\mathbf{i^{th}}$ element of the **DG** matrix is constructed by subtracting each new synthetic seismogram $\mathbf{S_n(Mo)}$ from the previous synthetic $\mathbf{S_n(Mo)}$. Thus the elements of the DG matrix are numerically obtained as explicit estimation makes the formulation. While computing the $\mathbf{S_n(Mo)}$ for the perturbation in the $\mathbf{i^{th}}$ element, the velocity of the $\mathbf{i^{th}}$ layer only

is perturbed by about 1 to 2%. Δm is the solution vector estimated using conjugate gradient method.

The problem is nonlinear and its success may depend on the proximity of the initial model to the true model. Here **DG**, Δm and Δd are $[m \times n]$, $[n \times 1]$ and $[m \times 1]$ matrices, respectively. We only invert for the S-wave velocity because the S-wave and surface waves, which are most sensitive to this velocity perturbation, are dominant in regional records. We then use the conjugate gradient method to solve for Δm [*Claerbout,* 1992]. The model perturbations Δm are added to the initial model $m_0^{(old)}$ for the new model $m_0^{(new)}$

$$m_0^{(new)} = \Delta m + m_0^{(old)}$$

The synthetics are computed using a reflectivity code that quickly computes the complete synthetic seismogram. The partial derivatives are computed using simple finite difference. We do not iterate on the residuals but instead recomputed the partial derivatives using the new model.

The method usually takes less than 10 iterations and requires a good initial model by a process of trial and error. We can invert multiple components and stations for a single event or multiple events depending upon the structure of the region, which must be near the 1-D model for the frequency band of interest.

Application to 1990 Cape Girardeau, 1991 Risco and 1991 Enola Earthquakes

We applied the above approach to three regionally recorded earthquakes within the Mississippi embayment region and applied the method to regional waveforms recorded at station CCM from the 1990 Cape Girardeau, Missouri, 1991 Risco, Missouri earthquakes (Figure 5 and 6). The source parameters for the 1990 and 1991 events were determined by *Langston* [1994] using a grid search scheme and velocity model calibrated from refraction and teleseismic receiver-function inversion. Although the receiver-function approach can resolve the deeper structure, it has poor resolution of the regional crustal structure. The source mechanism for the 2001 Enola event was determined using moment tensor inversion

of long period waves recorded at 10 stations and the depth using a grid search. With this many stations the long period moment tensor is well constrained but mismatches in phase and amplitude between the data and synthetics at shorter periods indicate that improvements can be made to the model. We inverted single station 3-component data and compared the results obtained for different paths to examine any azimuthal variations in earth structure.

The raw data were processed to displacement and the entire seismogram of reach of the three components was used. The long period P-waves are usually lower in amplitude and in the noise in regional records so we only invert for S-wave velocities. We computed synthetics by perturbing the S-wave velocity for only one layer at a time by about 0.1 km/s. The earth is parameterized as multiple layered medium with depth variations in S-wave velocities. We used a Poisson ratio of 0.25 to relate the P-wave velocities (α) to the S-velocities (β) and assumed a relationship of $\rho = 0.32\alpha + 0.77$ to constrain and densities (ρ) in order to limit the number of unknowns. This relation may not be appropriate for the shallow sediment structure. For the Cape Girardeau event we found, using synthetic tests, that the lower crust was poorly constrained and insensitive to the S-velocity perturbations. We therefore represented the entire crust between 25 and 40 km depths by a single layer to prevent trade-off between the surface layer and lower crustal layer velocities. The layer thicknesses were fixed but the thicknesses could vary with depth depending on the resolution for that layer depth. Low velocity surface layers can also be added to better fit the surface wave train. The data and synthetic waveforms were bandpassed using a 3-pole Butterworth acausal filter between 100 or 50 and 10 or 5 seconds period. We normalized the data and synthetics before the inversion for the vertical and horizontal components to have even weights. The tangential component was weighted strongly when the station receiver azimuth was near nodal.

The above inversion resulted in an improvement of the arrival time and amplitude of the major phases Sn, Sg, SmS, and Rayleigh waves which could not be observed using the initial model. The propagation paths from events 1 and 2 to the station CCM indicate that the average crustal velocity is between 6.2 and 6.5 km/s with a high velocity layer at 10 km depth and a low velocity zone (LVZ) at 25 km depth. The CCM record for event 2 also resolves a

gradual gradient from 5.5 to 7 km/sec from 25 to 40 km with upper mantle velocity of 7.8 km/sec. This is poorly constrained for the path from the event 1 although the average velocity for that layer is the same. By introducing a gradient along this path neither worsens nor improves the fit to the data. These models are in good comparison to the station CCM receiver function inversion by *Langston* [1994] although the LVZ and high velocity lid in the upper crust is not present in the receiver function result. Event 2 also traveled more through the embayment relative to event 1 so we add a low velocity surface layer to better fit the synthetics which is not needed in event 1.

Lateral Crustal Structure

The lateral heterogeneity of the Mississippi embayment structure has recently been delineated (Dart and Swolfs, 1998 and Mooney and Andrews, 1984), based on much drill-hole data from the upper Mississippi Embayment (Dart, 1992) and COCORP deep reflection profiles across the buried Reelfoot rift (Nelson and Zhang, 1991). In the neighboring Wabash Valley region, new evidence on paleoearthquakes has emerged from liquefaction data (Obermier *et al*., 1992). A special issue of SRL (July/August, 1997) on the Illinois basin contains several articles providing useful data on the basement structure of the Wabash Valley Seismic Zone (WVSZ). We have been compiling the seismic, geologic and geophysical data available from such sources for integrating into a first-order 3D velocity model of the embayment region in the New Madrid region extending into the Wabash Valley source region. Here, we plan to constrain ground motion characteristics within and around the Mississippi embayment and evaluate the effects of the embayment structure on wave propagation by analyzing the response of irregular basement structure using 3D finite-difference calculations. The initial structure model is prepared based on the contour maps of the relic structure in the Precambrian basement of the Reelfoot rift (Dart and Swolfs, 1998) which is based on a combination of new detailed depth-to-basement data in the Reelfoot rift (the lower left rectangle in Figure 1) and less detailed basement and outcrop data in the surrounding region. As new useful and critical data become available, we plan to incorporate them and modify the initial model. We also have a preliminary 3D basement map for a portion of the Wabash Valley (the upper right rectangle in Figure 1, Bear *et al.*, 1997) which is also a site of large paleoearthquakes (Obermier *et al*., 1993).

The principal feature of the Mississippi Embayment crust is the uplift of the deep crustal layers and the thinning of the upper crust. Earlier seismic refraction studies conducted by the U.S. Geological Survey in 1980 in the northern Mississippi embayment (Mooney *et al*., 1983; Ginzsburg *et al.*, 1983) show the variation of deep crustal structure of the northern Mississippi Embayment along and across the Reelfoot rift. Features of the shallow structure such as the sub-basins (SB), and major and minor structural highs that lie within upper and lower intra-rift basins are also crucial for understanding waveguide effects. Our current effort is primarily to assemble all this information together to develop the desired 3D model of the Embayment structure.

Influence of the Lateral Mississippi Embayment Structure on Regional Seismograms

(a) Analysis of the 2D Structure from Saint Louis to Memphis

To investigate the variation of seismic waveforms as caused by the variation in the crustal structure, we have simulated finite-difference seismograms using a crustal structure across the New Madrid rift complex (NMRC, Braile *et al*., 1997), extending from Memphis, Tennessee to the east of Saint Louis, Missouri. The USGS acquired refraction data for this approximately 400 km long profile which was investigated by Catchings (1999) to investigate the regional Vp, Vs, Vp/Vs and Poisson's ratios along the path. This later study yielded an extensive 2D velocity profile from Memphis to Saint Louis, which is inclusive of mini basins along the surface for the entire path. The path incorporates the Illinois basin too (Figure 7).

The model discretized in this study extends 400 km along the path from Memphis to Saint Louis and extends to a depth of about 55 km with a grid spacing of 200 meters. Next, we have used an event with a dip and rake of 70° and 30° respectively, a rise time of 2s and a f_{max} of 1.4 Hz to compute finite-difference seismograms with a source buried within the upper crust at a depth of 6 km -- 20 km off of both ends of the model. For each source, the first receiver is located 30 km from the end and interspersed equally to a distance of 380 km. Anelastic attenuation was represented by $Q_{á}$ of 400, 500 and 800 for the upper, middle and lower crust, respectively. No distinction was made in Q properties for the uppermost and

upper crust. Two possible cases of lateral crust were analyzed. First, we generated finite-difference seismograms using the lateral path model, which includes the middle crust and part of the lower crust to ensure that no seismic energy is reflected back from the moho discontinuity. The second crustal model incorporated structure below the moho discontinuity.

We used recent computation finite-difference algorithm and executed on a SUN workstation (Graves, 1998; Pitarka, 1999). Figure 8 shows the vertical and radial seismograms for the two cases discussed above for the source located near Memphis. Note the strong phases that are present at receivers from 1 (r=10 km) to 8 (r=80km) which reduce in strength until the receiver 30 (r=320 km). The seismograms in Figure 8a are for the case that does not include the moho discontinuity. We observed only subtle differences when these seismograms are compared these with those shown in Figure 8b (includes the moho discontinuity) except for the body waves preceding the surface waves at receivers located beyond 320 km. As the model extends from Memphis to Saint Louis, the upper crust starts to thin near Dexter (New Madrid) toward Saint Louis. Clearly this thinning of the structure seems to extend the duration of the surface waves at receivers lying directly above. We really do not see much difference in the waveforms shown in Figure 8a and Figure 8b except for a marginal change in peak amplitude. However, there are some recognizable differences in waveforms computed for the source located near the Illinois basin in the middle crust (Figure 9). In this case, the waveforms at receivers 36 (r=10km) to 29 (r=80 km) are not as strong as those in Figure 8(a,b) or receiver 1 to 8 where the source was buried within the upper crust and significant waves were reflected from the upper crust discontinuity. We also notice differences in the finite-difference seismograms computed for the two models. The S body waves are stronger over a longer period and total durations of the surface waves are also extended for the receivers within the Memphis region when the moho discontinuity is included. In addition, the attenuation is different for the source located near Illinois basin which remains flat compared to the case when seismic energy propagates from Memphis toward Saint Louis.

(b) 3D Mississippi Embayment Structure

Velocity Model Parameterization

The area covered by the FD simulations is depicted in Figure 1. This area was chosen to include the central part of the Mississippi embayment and the entire fault plane considered in the simulation of scenario earthquakes. The Mississippi embayment is composed of unconsolidated sediments overlying Paleozoic rocks. Its structure has been the object of several studies (e.g. SRL, 1997 July/August, special issue; Dart and Wolfs, 1998; Mooney and Andrews, 1984). The lateral variation of the embayment has been delineated based on drill-hole data (Dart, 1992) and COCORP deep reflection profiles across the buried Reelfoot rift (Nelson and Zhang, 1991). We used these data in the process of preparing a preliminary regional 3D velocity model.

In making the velocity model we focused mainly in generating the background 1D structure, geometry of the basement and shear-wave velocity of the unconsolidated sediments that occupy the shallow part of the model. The background 1D crustal structure was derived using the inversion method presented in the previous sections. The inverted model was calibrated using three regionally recorded earthquakes within the Mississippi embayment region. The inversion resulted in an improvement of the arrival time and amplitude of the major phases Sn, Sg, SmS, and Rayleigh waves, which were not produced by the initial model. Based on the inversion results the average crustal velocity is between 6.2 and 6.5 km/s with a high velocity layer at 10 km depth and a low velocity zone (LVZ) at 25 km depth. The CCM record for event 2 also resolves a gradual gradient from 5.5 to 7 km/sec from 25 to 40 km with upper mantle velocity of 7.8 km/sec. Our 1D crustal model is in good agreement with the CCM receiver function inversion by *Langston* [1994] although the LVZ and high velocity lid in the upper crust is not present in the receiver function result.

The shallow part of the model is prepared based on contour maps of the relic structure in the Precambrian basement of the Reelfoot rift (Dart and Wolfs, 1998) and physical parameters of the sedimentary basin obtained by Chen *et al*. (1996). In their shallow structure investigation Chen *et al*. (1996) used S-to-P converted waves recorded by 40 three-

component Portable Array for Numerical Data Acquisition (PANDA) stations deployed in the central New Madrid zone. The estimated shear-wave velocity of the sediments in the NMSZ varies from 0.45 to 0.67 km/sec. The region of higher shear-wave velocity is closely related to thicker sediments. The representation of small-scale variations of the velocity in the Quaternary layer in our model requires a very fine grid with spacing in the order of ten meters. Because of its extremely large computational requirement such a dense grid is not practical for wave-propagation modeling using available numerical techniques. In the velocity model we tested, the minimum grid spacing is 500 m, and the unconsolidated deposits are represented by a single layer with a minimum shear-wave velocity of 0.5 km/s. For this layer we assumed Vp = 1.8 km/s, density = 1.9 g/cm3 and Q = 50. Our simple parameterization of the sedimentary layer needs further improvements especially in the basins where the shallow structure is more complex.

Figure 10 shows contour-lines of basement depth and the fault location. A vertical cross section of the top 4 km of the 3D velocity model across a NW-SE direction is shown in Figure 11. The location of the profile is indicated by the blue line in Figure 10. The velocity contrast between the basement and the basin sediments, and the geometry of the basin edge in this area are key features of the basin structure that generate basin secondary waves. These waves mostly affect the waveform and duration of the ground motion at basin sites.

Source Parameterization of Scenario Earthquakes on the New Madrid Fault Zone

We calculated long period ground motion (periods longer than 2sec) for four M_w7.5 scenario earthquakes on the New Madrid fault zone. The fault, which is assumed to be the vertical and of predominantly left-lateral strike–slip type, runs through the central part of the Reelfoot rift. Its location is shown in Figure 10. We assumed that the fault ruptures along three vertical segments with different strike angles. The fault is 198 km long and 15 km wide. Its parameters are given in Table 2. The fault geometry and location were derived based on the recent seismic activity in the area (SRL, July/August, 1997).

As recognized by theoretical investigations and observations the distribution of slip on

the fault and rupture directivity may have a significant influence on the near-fault ground motion. For this purpose in our simulations of four scenario earthquakes we used two slip models characterized by multiple asperities and two different rupture nucleation points. The slip models were selected among several slip scenarios generated for an M_w 7.5 earthquake using a procedure developed by Abrahamson (1997, personal communications) based on Somerville *et al*. (1999). One of the slip models is shown in Figure 12.

The seismic moment for all scenario earthquakes was 2 x 10^{27} dyne cm, which corresponds to a M_w of 7.5. The rise time of about 3 sec was estimated using the empirical relation between the seismic moment **(Mo)** and the slip rise time **(T_r)** of Somerville *et al*. (1999) derived for moderate and large earthquakes.

$$\mathbf{T_r = 2.03 \times 10^{-9}\ Mo^{1/3}}$$

The slip velocity in each subfault is considered variable and is given in two time windows, which are separated by 1 sec. The variability of the slip is realized by defining the amount of slip allowed only in the strike direction. As demonstrated by Graves (1998) the representation of the source time function using multiple time windows has a significant impact on the amplitude of the simulated ground motion because it tends to minimize the artificial constructive buildup of long period energy associated with single time window and regular shape slip velocity representation.

Simulation Result

The simulation was performed using the finite-difference method of Pitarka (1999) using a regular grid. The minimum grid spacing of 500 m insured accurate calculations of the wave-field up to a frequency of 0.5 Hz. The results of simulations using two different rupture nucleation points for the two slip models are shown respectively in Figures 13-16. Each panel shows the distribution of the peak velocity for the three components of motion. The contour of the basin edge and the fault projection on the free surface are also shown. Note that in most of the scenarios the largest ground motion is concentrated along the fault area in the direction of rupture. The peak ground motion corresponds to direct shear-waves. It is important to

notice that, due to rupture directivity effects, rupture scenarios of shallow slip give larger long-period ground motion compared with those of deep slip. Also the fault segmentation breaks down the directivity effect along the fault which otherwise could have been more pronounced at near fault sites.

In order to identify the most important phases seen in the simulated ground motion in Figures 17 and 18 we show profiles of synthetic seismic sections calculated at stations along N-S arrays across the basin located 60-90 km east of the model origin. The locations of the stations arrays are shown in Figure 10. The synthetic velocity seismograms correspond to the scenario earthquake with shallow slip, and rupture nucleated in the western part of the fault (see Figure 13 for peak velocity distribution). The waveform at receivers located in the basin is complex. It is dominated by two long period pulses originated from the large asperities in the central and western part of the fault. In both seismic sections we can clearly see three types of waves: the direct wave, followed by the wave reflected from the basement, followed by the coda waves which are mainly secondary surface waves generated at the basin edge, but also include multiple reflections within the basin sedimentary layers. The ground motion at rock sites is dominated by the direct S wave which is polarized in the direction almost normal to the fault, while at the basin sites the largest ground motion corresponds mainly to the direct S-wave or basin reflected waves propagating vertically. The rupture directivity creates a zone of large ground motion along the extremities of the fault. The easterly extent of this zone depends on the location of the rupture nucleation and the closest asperity. The worst scenario is the one shown in Figure 13 that has a large asperity and rupture nucleation located near the center of the fault. The largest amplification is observed in basin sites where the rupture directivity is strong for rupture initiation at either the eastern or western ends of the fault. The ground motion amplification in these areas is also strongly affected by the velocity contrast between basin sediments and bedrock.

Our simulations indicate that there are no strong 3D wave propagation effects at basin sites in the considered frequency range. This is due to the fact that the basin is very shallow. Moreover our model assumes homogeneous structure for the basin sediments. The predominant effect of the basin is trapping of energy within the sedimentary layer which

causes the increase in ground motion duration. Although the probability that an earthquake of similar magnitude is produced by faults adjacent to the basin edge is low, we considered a fifth scenario earthquake generated by a single segment fault located along the northern edge of the basin. The results of the simulations are shown in Figures 19-21. As suggested by the peak velocity distribution the large ground motion is associated with the direct wave. The peak amplitude (Figure 19) is mainly affected by the rupture process. As indicated in Figures 20 and 21 the ground motion at sites near the basin edge is dominated by basin edge generated waves. Due to the very strong velocity contrast between the bedrock and basin surface sediments, the amplitude and duration of these waves is relatively large.

Investigations of the basin edge effects indicate that the strength and extent of the amplification zone caused by the interference and focusing of basin edge induced waves at sites close to the basin edge depends on the basin edge geometry and depth (e.g. Pitarka *et al*., 1998)

Based on these results we conclude that the potential for amplification due to the basin edge effect is high only in areas along the basin margins and for earthquakes on faults located near the basin edges. In the central part of the basin the ground motion is dominated by basin reflected waves. Due to the limited geological and geotechnical information, the shallow part of the basin structure is poorly resolved. Ground motion modeling of local events is necessary to check the validity of the 3D basin model in this region.

Amplification Function Using Basin Response and Site Response

All of the available ground motion attenuation models for the central and eastern United States are for a hard rock ground surface, with a surface shear wave velocity of 2.83 km/sec. The average shear-wave velocity of the top surface layer at basin sites in our velocity model of the Mississippi Embayment is about 600 m/s. This corresponds to the shear-wave velocity of soft sedimentary rock. Based on our 3D ground motion simulations we developed a ground motion amplification function for basin sites that converts ground motion on the surface of hard rock to ground motion on the surface of the soft sedimentary rock of the

Mississippi Embayment at basin sites with depth to basement deeper than 500m.

The amplification function that we developed addresses two effects. The first is the effect of the impedance contrast between hard rock and soft rock, due to the contrast in shear wave velocity and density. The second effect is the development of surface waves that are trapped within the sedimentary rock of the Mississippi embayment.

To quantify these effects at periods longer than two seconds, we performed pairs of simulations of ground motions for the considered scenario M_w 7.5 earthquakes occurring on the New Madrid Seismic Zone. One simulation used a flat layered hard rock crustal structure with a surface velocity of 2.83 km/sec. The other simulation used our 3D velocity model of the Mississippi Embayment. Both models include rock damping, which is much larger in the sedimentary rocks of the Mississippi Embayment than in the underlying basement rocks.

Ground motion calculations were done for the four different earthquake scenarios, at a set of 24 locations within the Mississippi Embayment where the depth of the Embayment is more than 0.5 km. The amplification function was obtained by taking the ratio of Mississippi Embayment to hard rock motions at each of the 24 stations for each of the four earthquake scenarios, and averaging these ratios. This amplification function is expected to be representative of the amplification at sedimentary soft rock sites for large earthquakes occurring within the New Madrid Seismic Zone for periods longer than 2 seconds.

The three dimensional deep structure of the Mississippi Embayment is expected to have little impact on the ground motion amplitudes for periods of two seconds and shorter. The amplification at these periods was estimated by calculating the transfer function of a 1D model of the Mississippi Embayment, listed in Table 3. The upper four layers of this model represent the sedimentary rocks of the Mississippi Embayment. The rock damping of the layers of the model are represented by the inverse of the Q values of these layers. This damping is much higher in the sedimentary rocks of the Mississippi Embayment than in the underlying basement rocks.

When the amplification function for this 1D model was smoothed, it connected smoothly with the long period amplification function obtained from the ratio of the 3D Mississippi Embayment to 1D hard rock simulations. The amplification function is listed in Table 4. In the period range of 5 seconds to about 0.1 second, the amplification due to impedance contrast is larger than the deamplification due to rock damping effects, causing a net amplification. However, for periods shorter than about 0.1 second, the amplification due to impedance contrast amplification is smaller than the deamplification due to rock damping effects, causing a net deamplification.

Conclusions

Based on the modeling of regional seismograms recorded at station CCM from earthquakes at different locations in the Mississippi embayment, we were able to define the near-surface structure to provide a better fit in the arrival time and amplitude of the major phases Sn, Sg, SmS, and Rayleigh waves, an improvement relative to the previous models of the region. The propagation paths from the Cape Girardeau and Risco events to the station CCM indicate that the average crustal velocity is between 6.2 and 6.5 km/s with a high velocity layer at 10 km depth and a low velocity zone (LVZ) at 25 km depth. The CCM seismograms for the Risco earthquake were able to resolve a gradual gradient from 5.5 to 7 km/sec from 25 to 40 km with upper mantle velocity of 7.8 km/sec, which was poorly constrained for the Cape Girardeau event.

Our analysis of the two-dimensional finite-difference seismograms generated along the path from the city of Saint Louis, Missouri to Memphis, Arkansas indicates that as the crustal structure thins from Dexter to Saint Louis and as the seismic waves propagate towards the thin edge, the surface waves start to extend in duration for receivers that lie above the thin portion of the model. When the source is located towards the right edge of the model (Figure 7), the seismograms appear to have the features of those that can be simulated using a one-dimensional model.

Finally, we investigated the effect of the three-dimensional sedimentary structure of the Mississippi embayment due to a large earthquake in the New Madrid fault zone (Mw 7.5).

Within the limit of the frequency band (up to 2s), this study failed to yield any spectacular results that would be observed during such large scenario earthquakes that could not have been captured if we were to include only the one-dimensional aspects of the simulation where the effect of the impedance contrast is included (Saikia and Somerville, 1997; Somerville *et al.*, 1995).

ACKNOWLEDGEMENTS

Authors acknowledge Dr. J. A. Armbruster of Lamont Doherty Earth Observatory (LDEO) for providing waveforms used in this study. We also thank Dr. Jer Ming Chiu of the Center of Earthquake Research Institute (CERI) at Memphis University for providing his initial three-dimensional crustal model.

REFERENCES

Bear, G. W., J. A. Rupp and A. J. Rudmann (1997). Seismic interpretation of deep structure of the Wabash Valley, Seis. Res. Lett., 68, 624-640.

Braile, L. W., W. J. Hinze, and G. R. Keller, (1997). New Madrid seismicity, gravity anomalies, and interpreted ancient rift structures, Seis. Res. Lett., 68, 599-610.

Catchings, R. D. (1999). Regional Vp, Vs, Vp/Vs and Poisson's Ratios across earthquake source zones from Memphis, Tennessee, to Saint Louis, Missouri, Bull. Seis. Soc. Am., 89, 1591-1605.

Chen, K.-C., J.-M. Chiu and Y.-T. Yang (1996). Shear-wave velocity of the sedimentary basin in the upper Mississippi Embayment using S-to-P converted waves. *Bull. Seism. Soc. Am.*, **86**, 84

Claerbout, J. F., Earth Sounding Analysis Processing Versus Inversion, Blackwell Scientific Publications, Boston, MA., 1992.

Dart, R. L. (1992). Catalog of pre-Cretaceous geologic drill-hole data from the upper Mississippi Embayment-A revised and Update, Open File Report 90-260, USGS Open File Rep., 92-685, 253p.

Dart, R. L. and H. S. Swolfs (1998). Contour mapping of relic structures in the Precambrian basement of the Reelfoot rift, North American mid-continent, Tectonic, 17, 235-249.

Ginzburg, A., W. D. Mooney, A. W. Walter, W. J. Lutter, and H. H. Healy (1983). Deep structure of northern Mississippi Embayment: Am. Assoc. Petr. Geol. Bull., 67, 2031-2046.

Graves, R.W., A. Pitarka, and P.G. Somerville (1998). Ground motion amplification in the Santa Monica area: effects of shallow basin edge structure, *Bull. Seism. Soc. Am*., **88**, 1224-1242.

Graves, R. W. (1998). Long period 3D finite difference modeling of the Kobe mainshock, ESG 1998, 2nd Intern. Symp. On the Effects of Surface Geology on Seismic Motion, 47-52.

Obermier, S. F., J. R. Martin, A. D. Frankel, T. I. Youd, P. J. Munson, C. A. Munson and E. C. Pond (1993). Liquefaction evidence for one or more strong Holocene earthquakes in the Wabash Valley of southern Indiana and Illinois, with a preliminary estimate of magnitude, USGS Prof. Paper 1536, 27p.

Olsen, K. B., and R. J. Archuleta (1996). Three-dimensional simulation of earthquakes on the Los Angeles fault system, *Bull. Seism. Soc. Am.*, **86**, 575-596.

Pitarka, A., K. Irikura, T. Iwata and H. Sekiguchi (1998). Three-dimensional simulation of the near-fault ground motion for the 1995 Hyogo-ken Nanbu (Kobe), Japan, earthquake, *Bull. Seism. Soc. Am.*, **88**, 428-440.

Pitarka, A, (1999) 3D elastic finite-difference modeling of seismic motion using staggered grids with non-uniform spacing, *Bull. Seism. Soc. Am.*, **89**, 54-69.

Langston, C. A., An integrated study of crustal structure and regional wave propagation for southern Missouri, *Bull. Seism. Soc. Am.,* 84, 105-118, 1994.

Saikia, C. K. and P. G. Somerville (1997). Simulated hard-rock motions in Saint Louis, Missouri from large New Madrid earthquake. Bull. Seis. Soc. Am., 87, 123-139.

Somerville, C. K. Saikia, D. J. Wald and R. W. Graves (1995). Implications of the Northridge earthquake for strong ground motions from thrust faults, Bull. Seis. Soc. Am., Vol. 86, S115-S125.

Somerville, P.G.,K. Irikura, R.W. Graves, S. Sawada, D. Wald, N. Abrahamson, Y. Iwasaki, T. Kagawa, N. Smith and A Kowada, Characterizing crustal earthquake slip models for the prediction of strong ground motion (1999), *Seismological Research Letters*, **70**, 59-80.

Xu, Y., and D. A. Wiens, Upper mantle structure of the southwest Pacific from regional waveform inversion, *J. Geophys. Res.,* 102, 27,439-27,451, 1997.

Table 1. Source Parameters of Events Used in this Study

OT	hr:mn:ss	Lat	Lon	h	M_w	Φ	δ	λ	Location
90.9.2	13:18:51.33	37.17	89.58	15	4.3	59	60	155	CG
91.5.1	01.18/54.19	36.56	89.82	8	4.2	88	64	-11	R
01.5.4	06:42:12.68	3.21	92.19	5	4.5	117	86	-32	E

CG=Cape Girardeau, MU; R=Risco, MO; E=Enola, AR

Table 2. Fault Parameterization

Fault Length	189 km		
Fault Width	15 km		
Depth to the Top	2 km		
Seismic Moment	$2. \times 10^{27}$ dyne cm		
Effective Rise Time	3 sec		
Rupture Velocity	2.9 km/s		
Subfault Dimensions	$11 \times 3 km^2$		
	Segment 1	Segment 2	Segment 3
Length	110 km	44 km	44 km
Width	15 km	15 km	15 km
Strike	40°	342°	40°
Dip	90°	90°	90°

Table 3. 1D Seismic Velocity Model of the Mississippi Embayment for use in Calculation of Transfer Function

P velocity (km/sec)	S velocity (km/sec)	Density (gm/cc)	Q	Thickness (km)
1.80	0.60	1.9	50	0.25
2.10	1.00	1.9	100	0.25
3.12	1.80	2.0	100	0.5
4.50	2.60	2.2	200	0.5
5.00	2.90	2.4	500	4.5
5.54	3.20	2.6	500	16.0

Table 4. Amplification Function for the Mississippi Embayment

Frequency	Period	Amplification
0.20	5.00	1.60
0.25	4.00	1.76
0.33	3.00	1.82
0.50	2.00	1.86
1.0	1.00	1.83
2.5	0.40	1.77
3.5	0.285	1.69
5.0	0.20	1.51
9.0	0.11	1.25
10.0	0.10	1.20
25.0	0.04	0.73
33.0	0.03	0.60

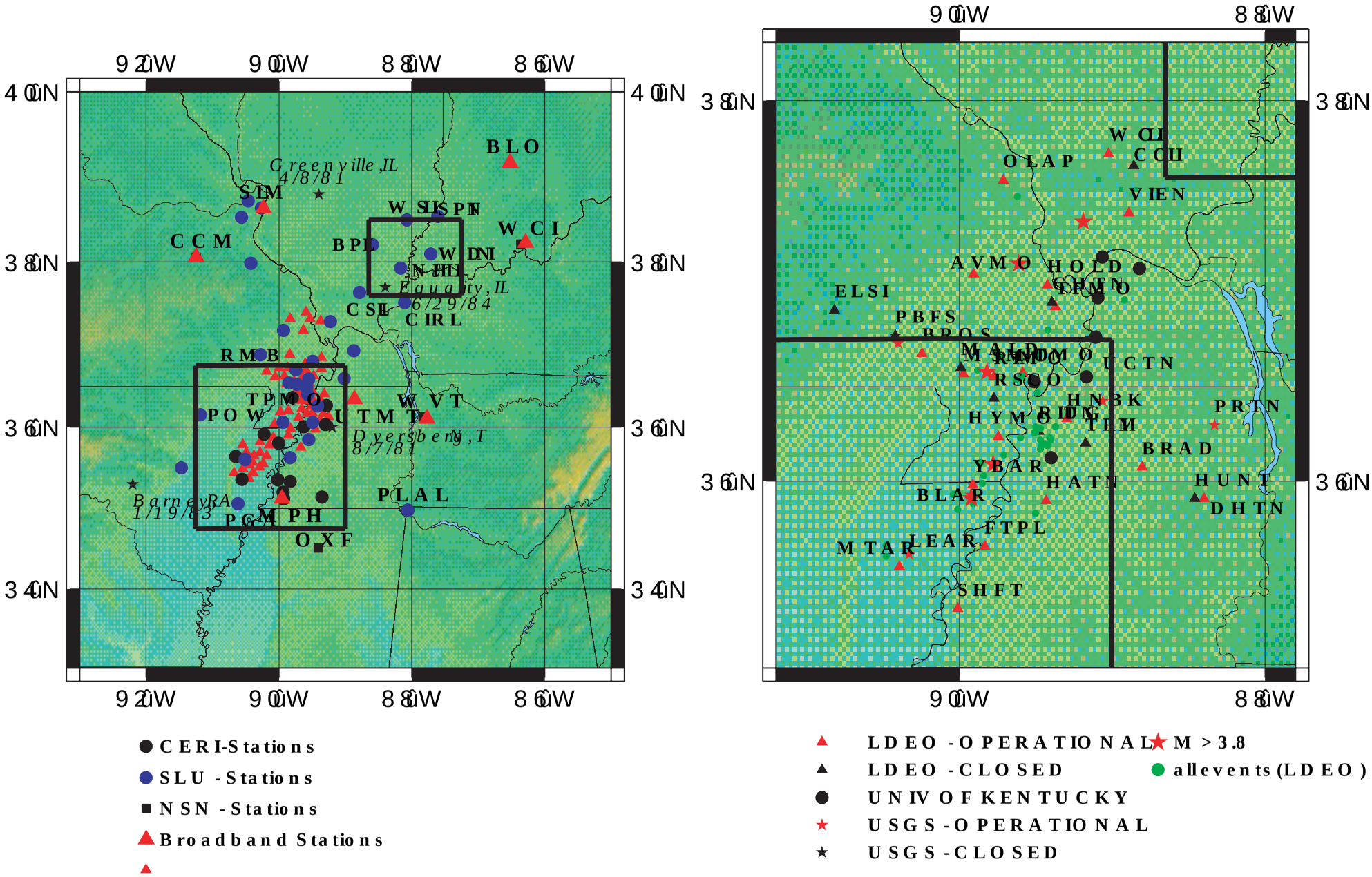

Figure 1. Maps showing locations of stations that operate (or operated) in the central United States. Left map shows locations of stations run by SLU, CERI, NSN (broadband) network. Note the coverage of other stations shown by the small red triangles. Right map is only for strong-motion stations. Also shown are the locations of large earthquakes (Mb>4, red large stars) and other events (green circles, for the period 1988-2000) that were recorded by strong-motion networks.

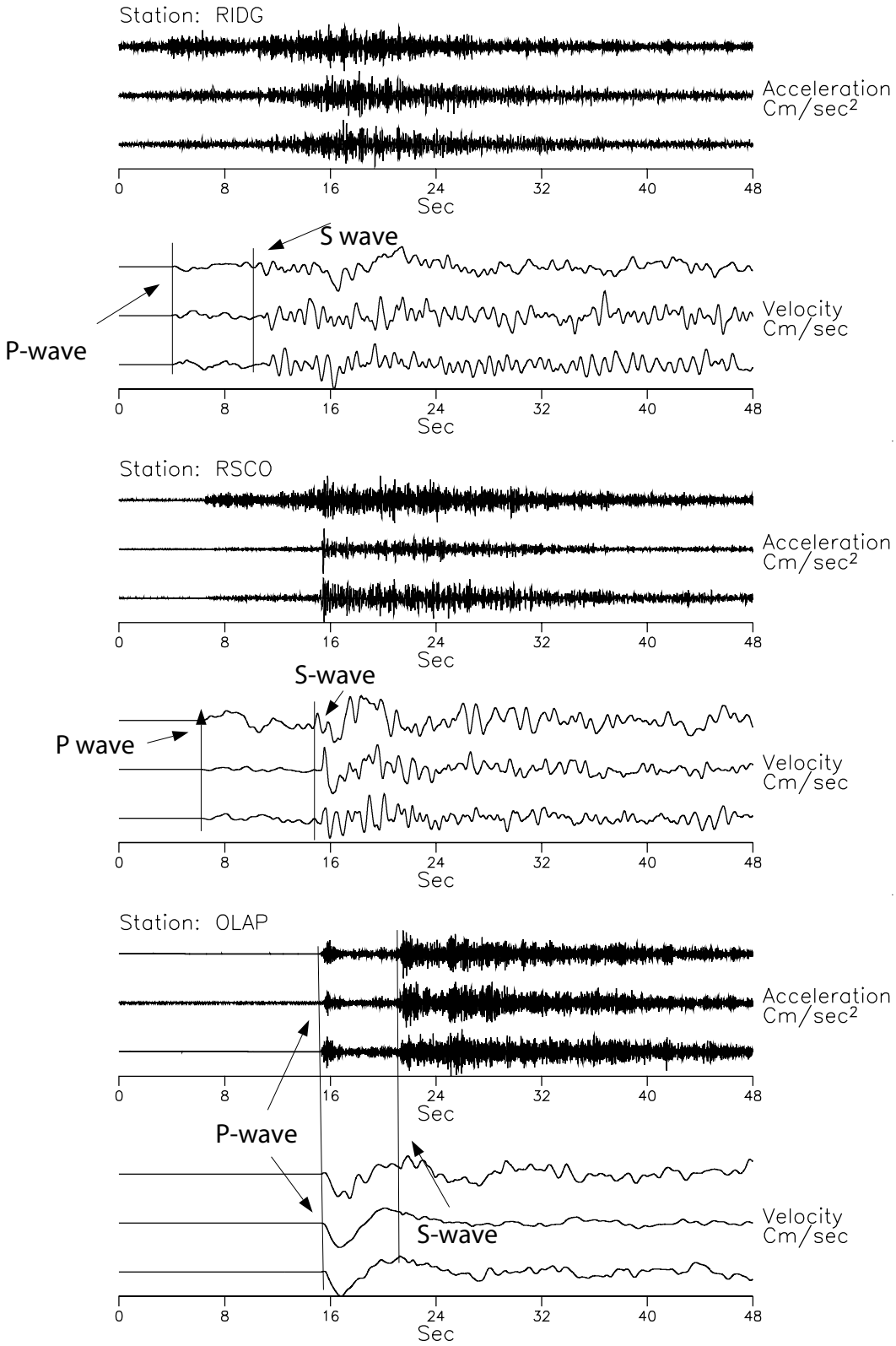

Figure 2. Examples of strong motion data recorded by three stations of the LDEO network from an Embayment earthquake (9/26/90, mb=4.7, 37.165N 89.577W, h=12 km). Both accelerograms and velocity seismograms are plotted. Note the differences in characteristics of the velocity seismograms.

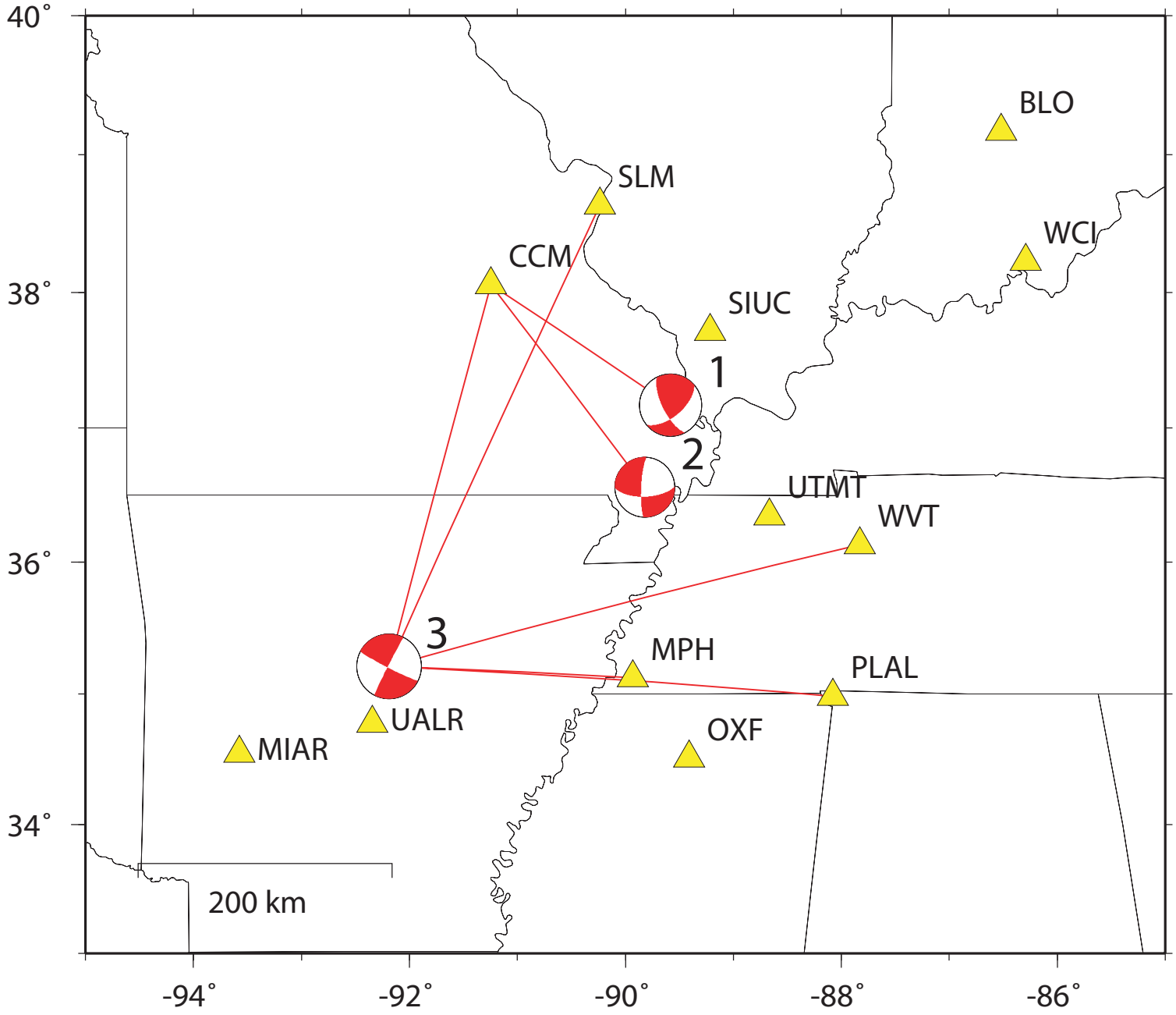

Figure 3. Map of Saint Louis, US National Network and IU broadband stations in the New Madrid seismic zone. We used long-period seismograms recorded at station CCM from the (1) 1990 Cape Girardeau, (2) 1991 Risco, Missouri and (3) 2001 Enola, Arkansas earthquakes to invert for the S wave velocity models, especially of the near-surface structure. In general, paths vary from one evenet to the other, thus indicating that the near surface sediimentary structure is laterally varying.

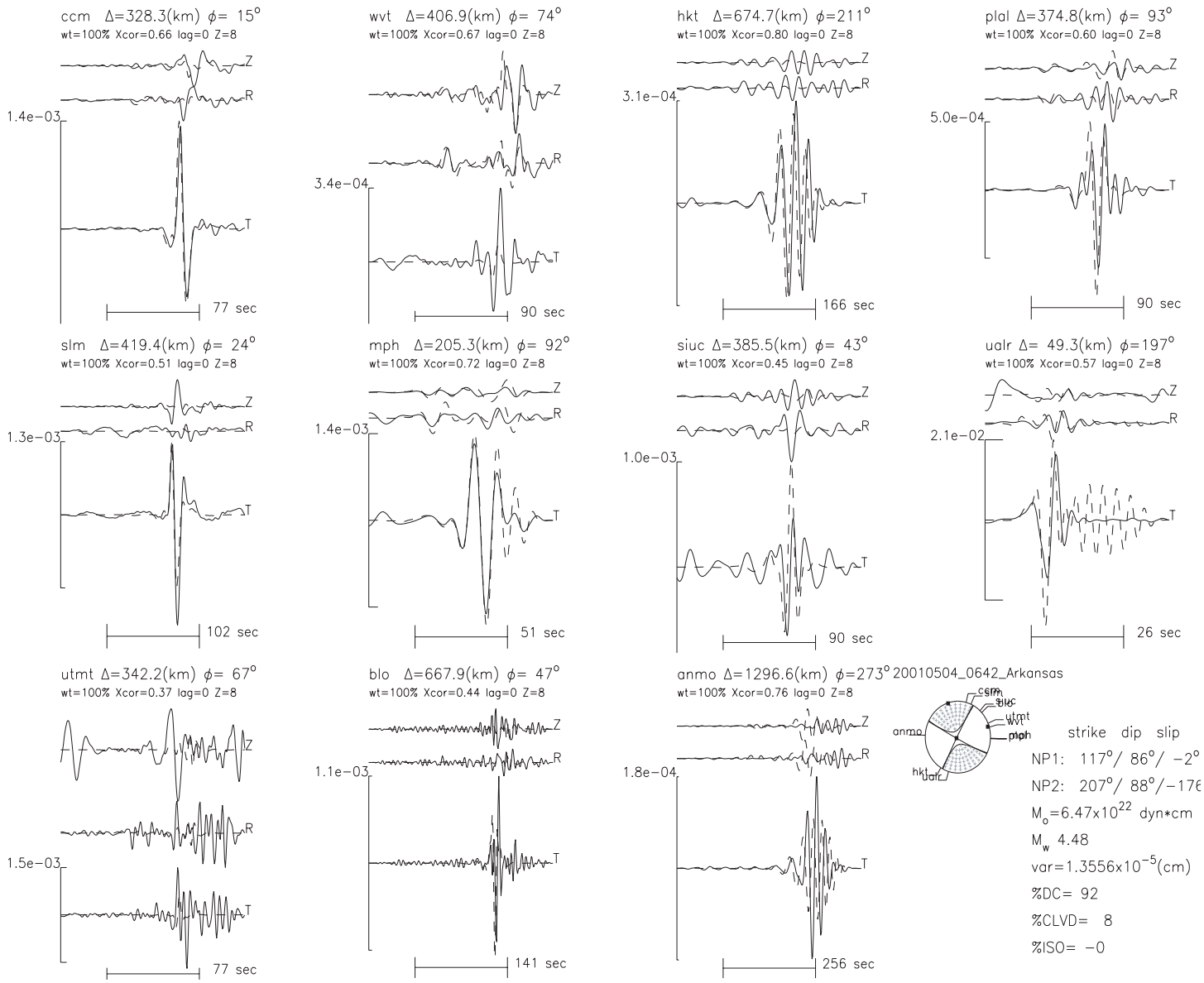

Figure 4. Modeling of the 2001 Enola, Arkansas earthquake. We used long-period data from several stations to invert for the moment-tensor solution of this earthquake and its depth. Note that for the majority of the stations the tangential motions are stronger than the other two components except for stations WVT, SIUC and UTMT. This study requires additional investigation in the modeling of the short-period features.

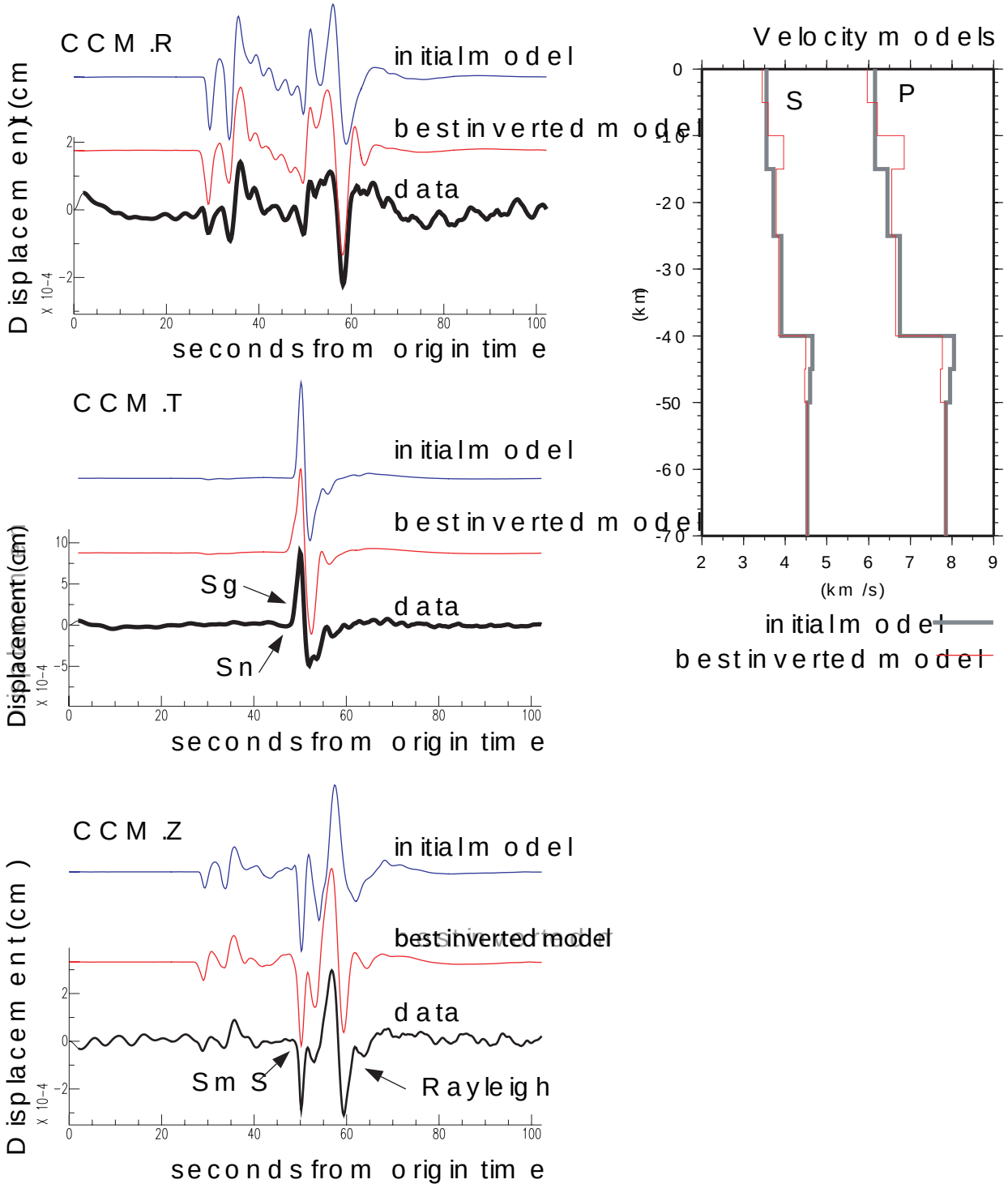

Figure 5. Comparisons between synthetic and observed 3-component displacement seismograms from the 1990 Cape Girardeau earthquake recorded at station CCM. We filtered the records between 5 and 50 second periods and inverted for the S-wave velocity model using the waveform inversion. The inversion converged to the final solution within three interations. The comparison shows considerable imporvement up to 5 seconds periods, especially for the Sn, Sg, SmS, and Rayleigh waves relative to the initial model.

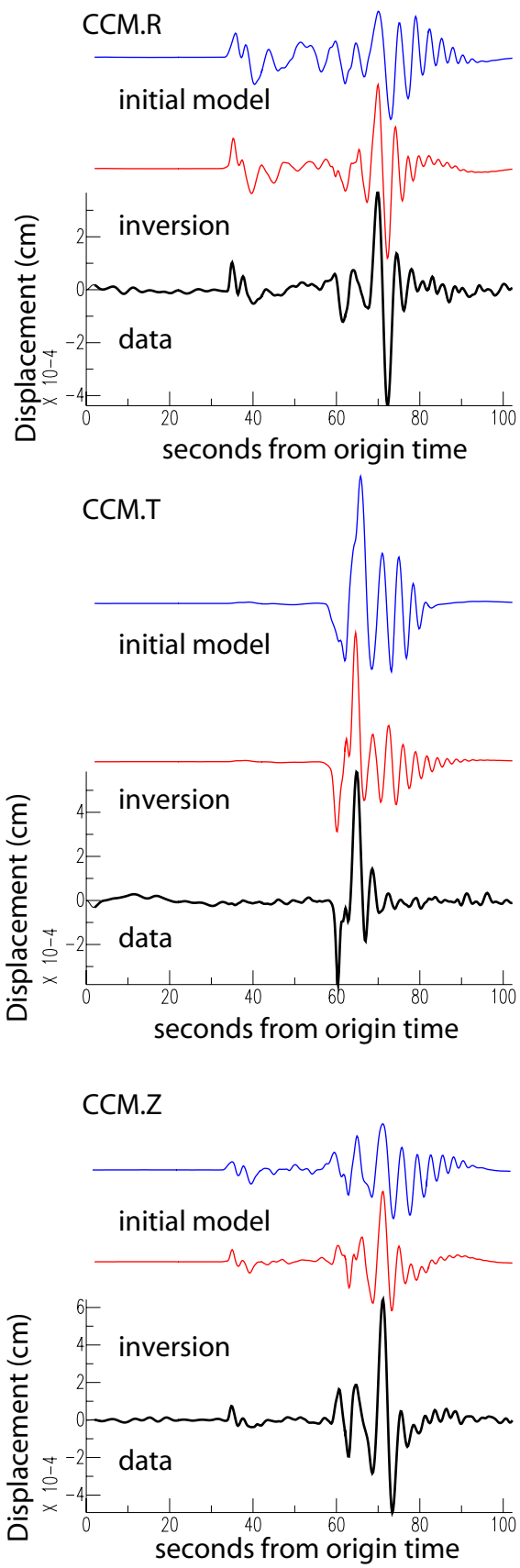

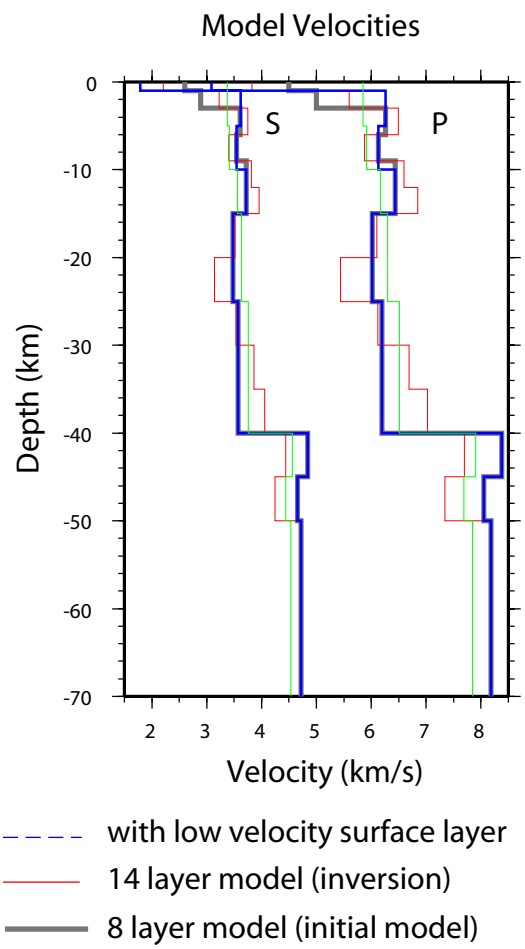

Figure 6. Comparisons of synthetic and observed three-component seismograms recorded at station CCM from the 1991 Risco earthquake. We filtered the recorded seismograms between 5 and 50s and inverted for the near-surface strcucture of the S-wave velocities. The inversion converged to the final solution within 8 iterations. We also inverted the data using a 8 layered velocity model with a low surface wave velocity layer which improved the match slightly.

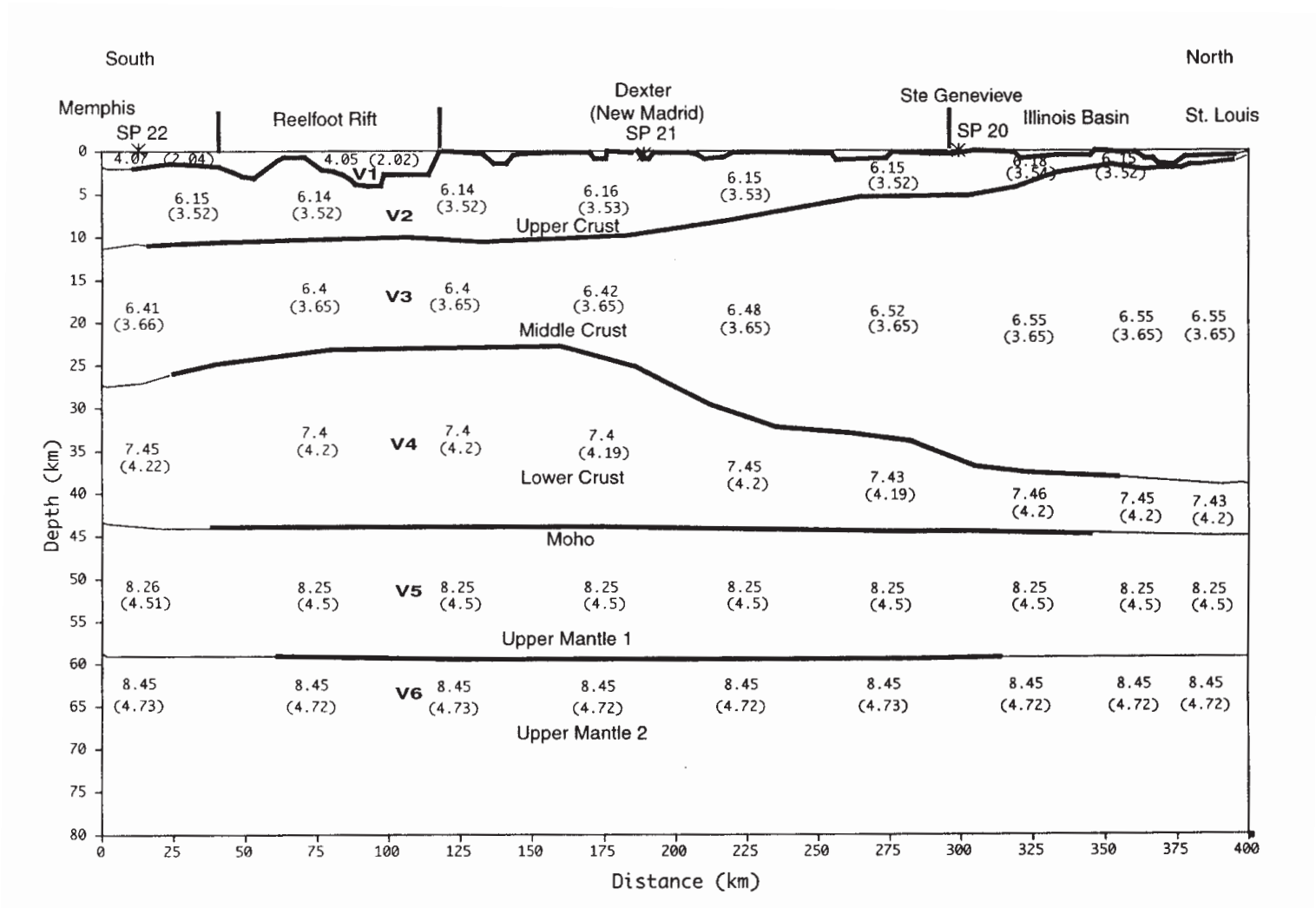

Figure 7. A velocity model of the Mississippi Emabayment from Memphis to Saint Louis. Vertical axis is for depth. Both axes are in kilometers. In our computation we use the entire path along the horizontal axis and include structure to a depth of about 55 km. The first receiver (1) is placed to the left of the model (near Memphis) 30 km off the model boundary.

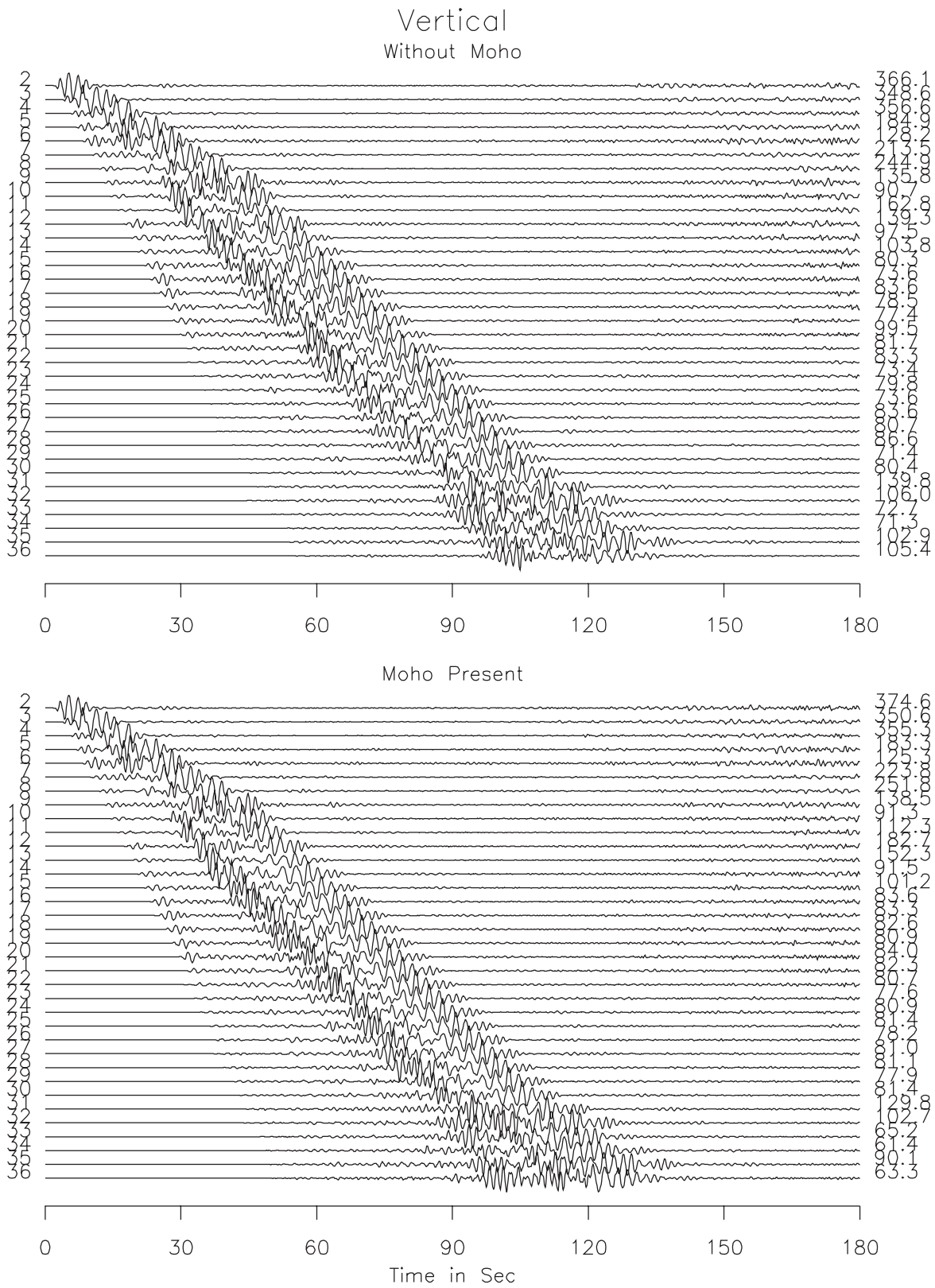

Figure 8a. Profile of the vertical component ground acceleration time histories generated using the two-dimensional structure shown in Figure 7. Seismograms shown in the top panel were computed using only the lateral structure near the surface; the moho was not included. We embeded the source at a depth of 6 km near a location underneath the city of Memphis and is 20 km off from the left edge of the model. The receiver of the uppermost seismogram is located 30 km off the left edge of the model also. The bottom panel shows the seismograms for the same scenario, but in this case the model included the moho.

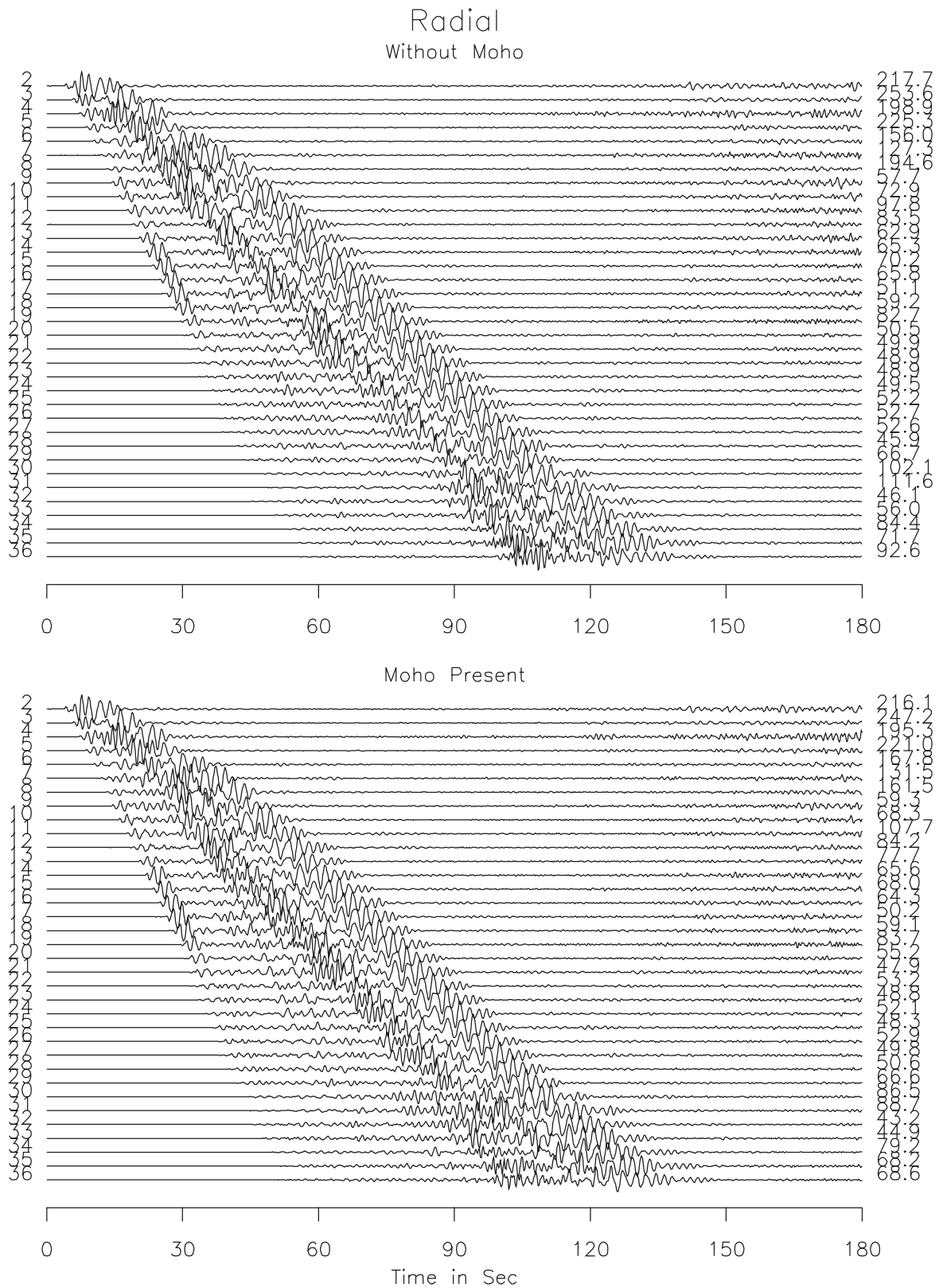

Figure 8b. Profile of the radial component ground acceleration time histories generated using the two-dimensional structure shown in Figure 7. Seismograms shown in the top panel were computed using only the lateral structure near the surface; the moho was not included. We embeded the source at a depth of 6 km near a location underneath the city of Memphis and is 20 km off from the left edge of the model. The receiver of the uppermost seismogram is located 30 km off the left edge of the model also. The bottom panel shows the seismograms for the same scenario, but in this case the model included the moho.

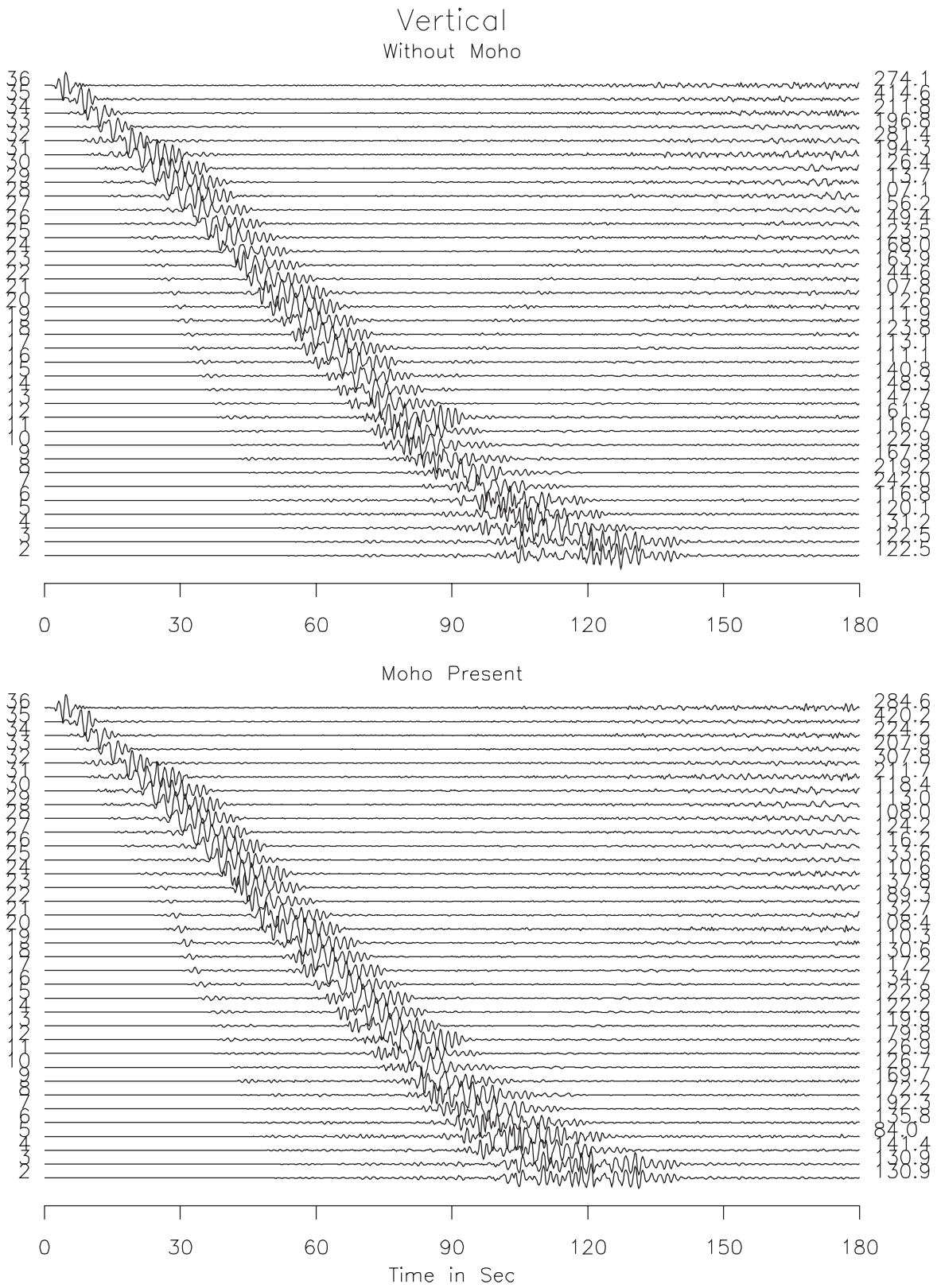

Figure 9a. Profile of the vertical component ground acceleration time histories generated using the two-dimensional structure shown in Figure 7. Seismograms shown in the top panel were computed using only the lateral structure near the surface; the moho was not included. We embeded the source at a depth of 6 km near a location underneath the city of Saint Louis and is 20 km off from the left edge of the model. The receiver of the uppermost seismogram is located 30 km off the left edge of the model also. The bottom panel shows the seismograms for the same scenario, but in this case the model included the moho.

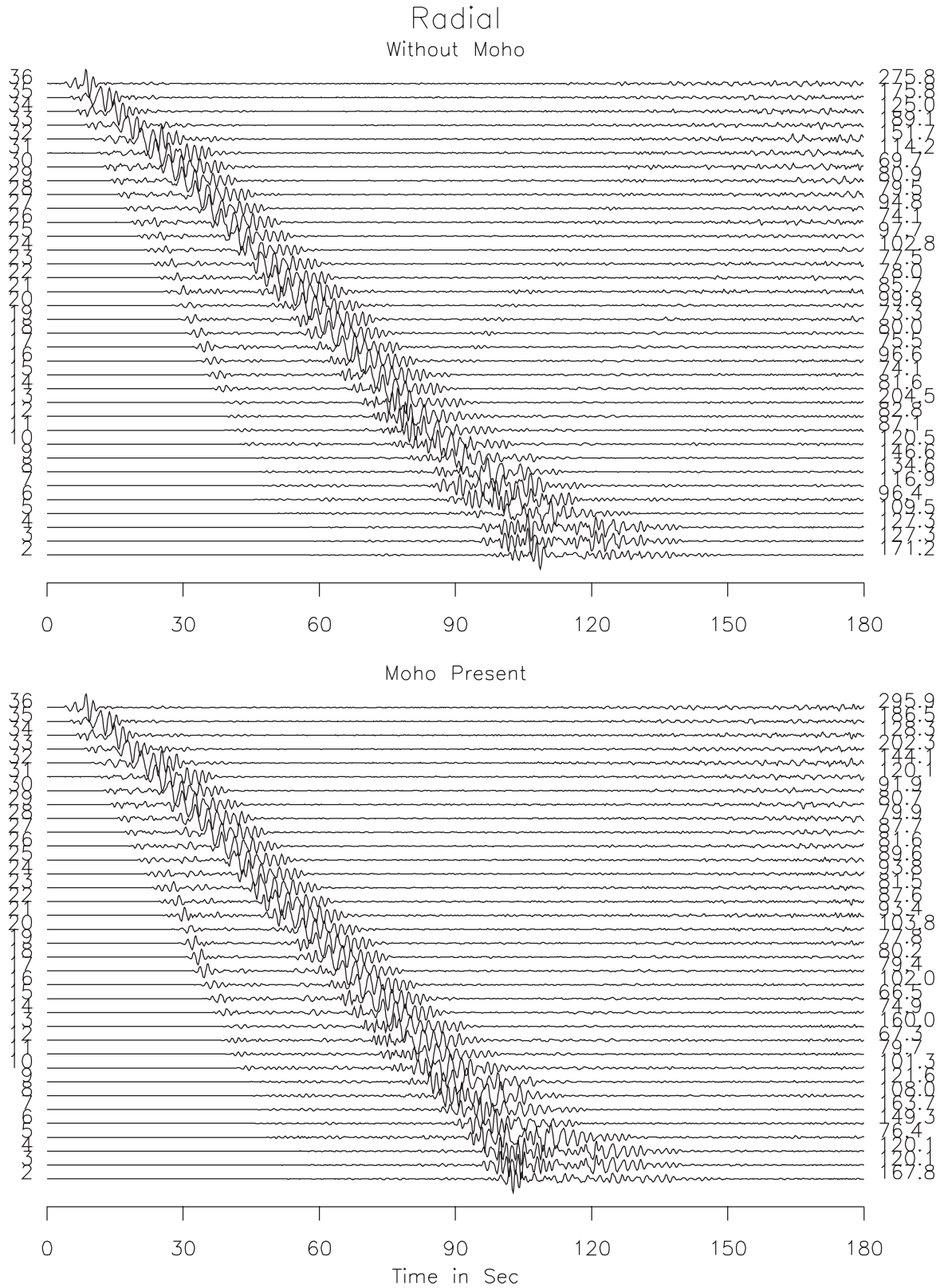

Figure 9b. Profile of the radial component ground acceleration time histories generated using the two-dimensional structure shown in Figure 7. Seismograms shown in the top panel were computed using only the lateral structure near the surface; the moho was not included. We embeded the source at a depth of 6 km near a location underneath the city of Saint Louis and is 20 km off from the left edge of the model. The receiver of the uppermost seismogram is located 30 km off the left edge of the model also. The bottom panel shows the seismograms for the same scenario, but in this case the model included the moho.

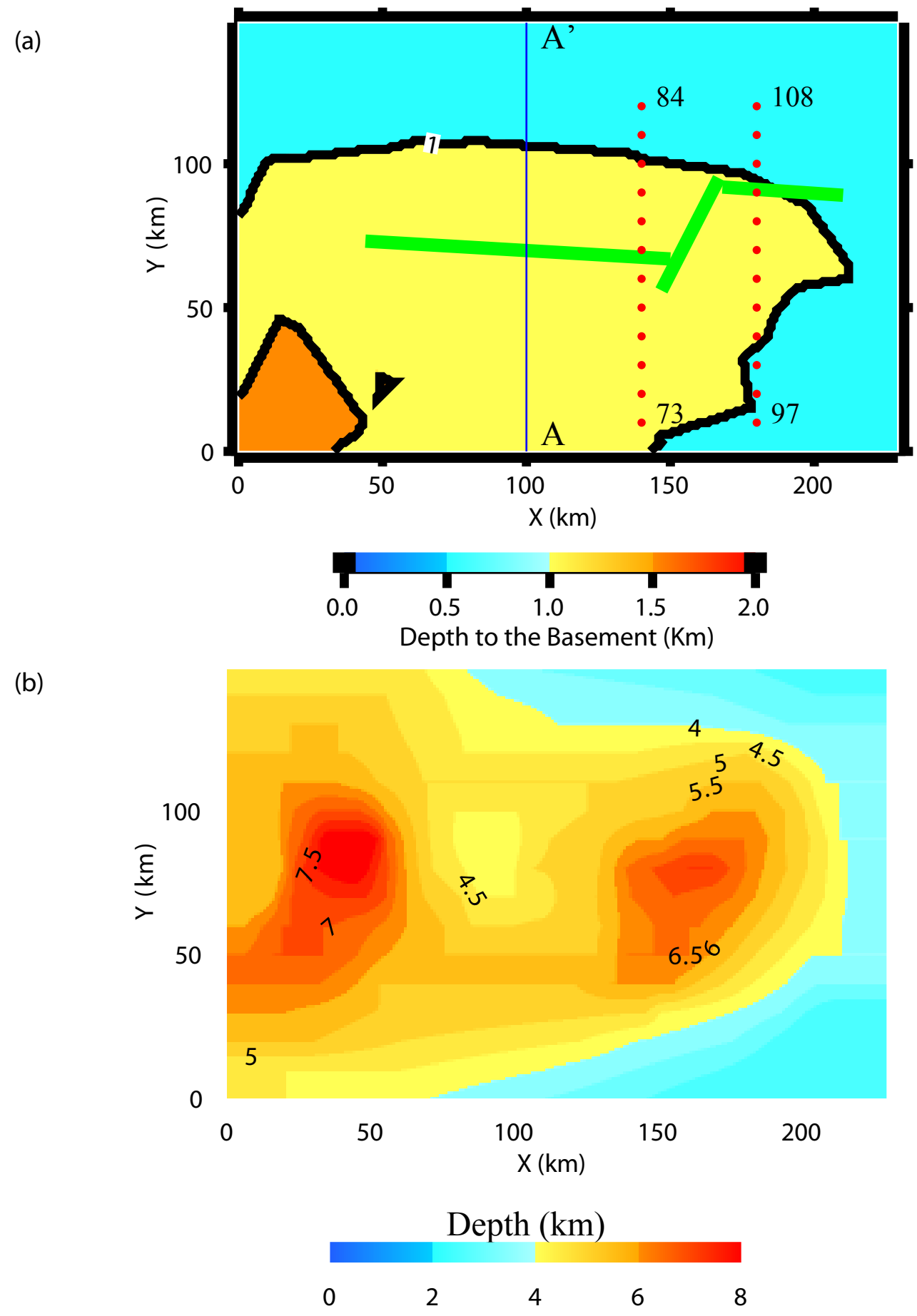

Figure 10. (a) Map of the depth to the isovelocity layer with Vs=2.9 km/s. Green line shows the fault projection to the surface. Blue line indicates the location of the velocity cross-section A-A'. Red circles show two lines of stations used in displaying seismic profiles. (b) Contours map of the Reelfoot rift basement showing the sub-basins within the upper and lower intra rift basin.

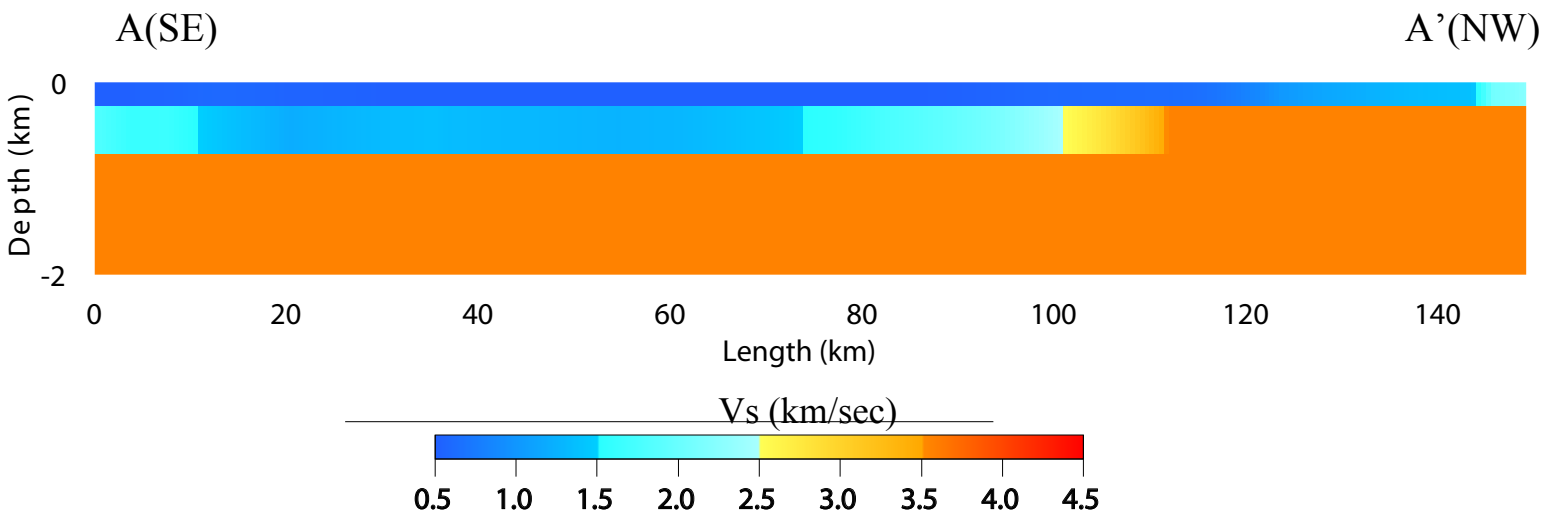

Figure 11. Cross sections of the 3D velocity model along SE-NW.

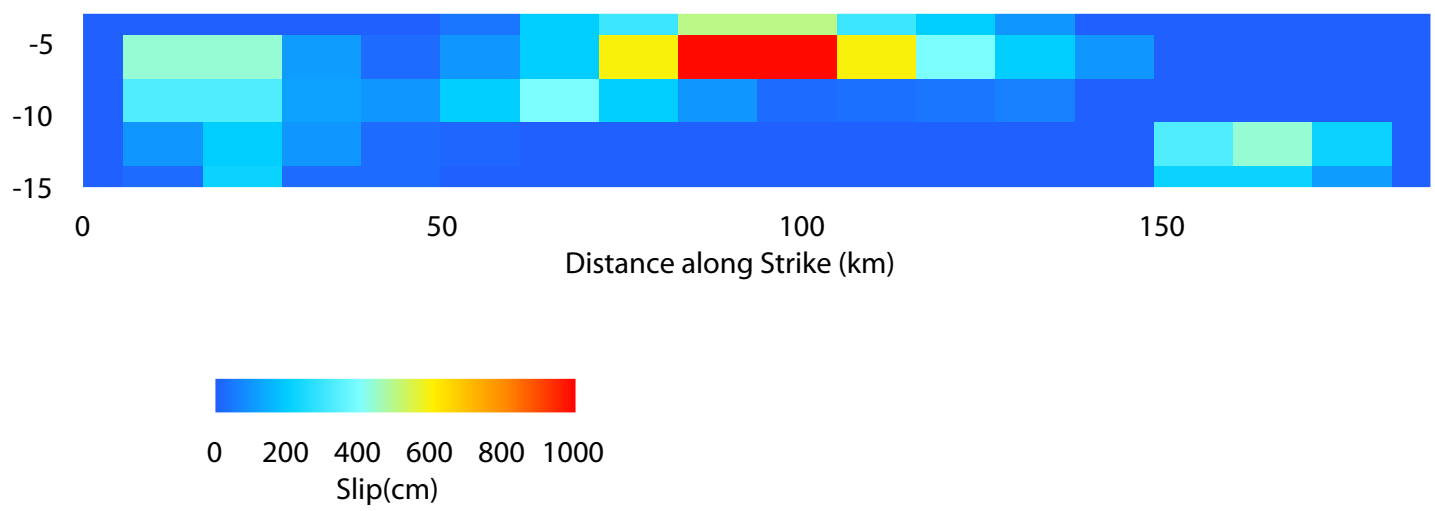

Figure 12. Slip model with shallow asperity used in one of the simulations.

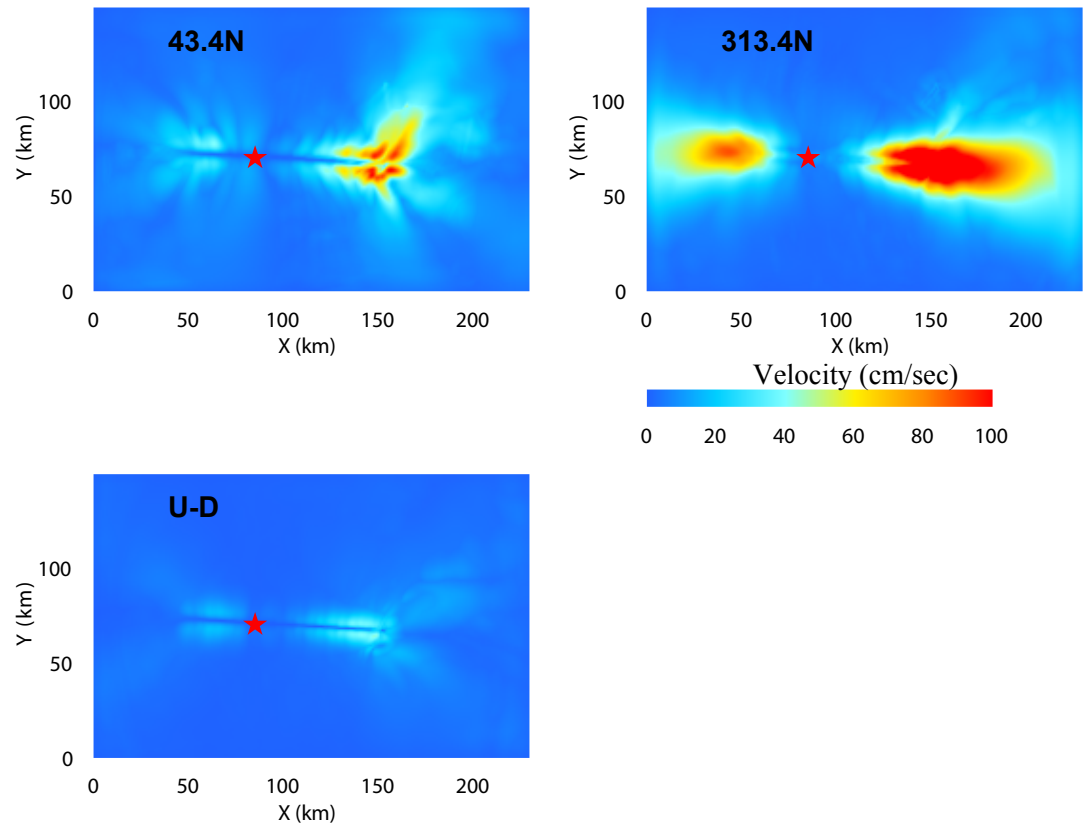

Figure 13. Peak velocity distribution obtained with the slip model with shallow asperity, and the hypocenter located on the west side of the fault. Star shows the epicenter locations.

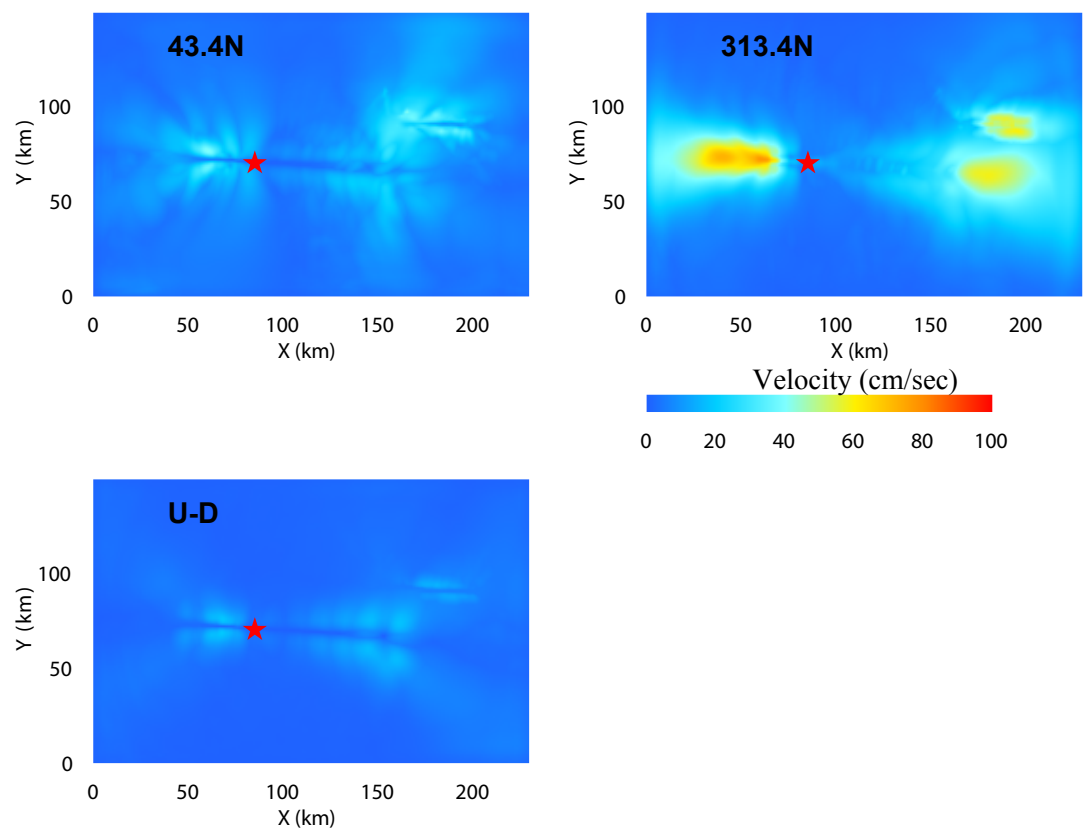

Figure 14. Peak velocity distribution obtained with the slip model with shallow asperity, and the hypocenter located on the east side of the fault. Star shows the epicenter locations.

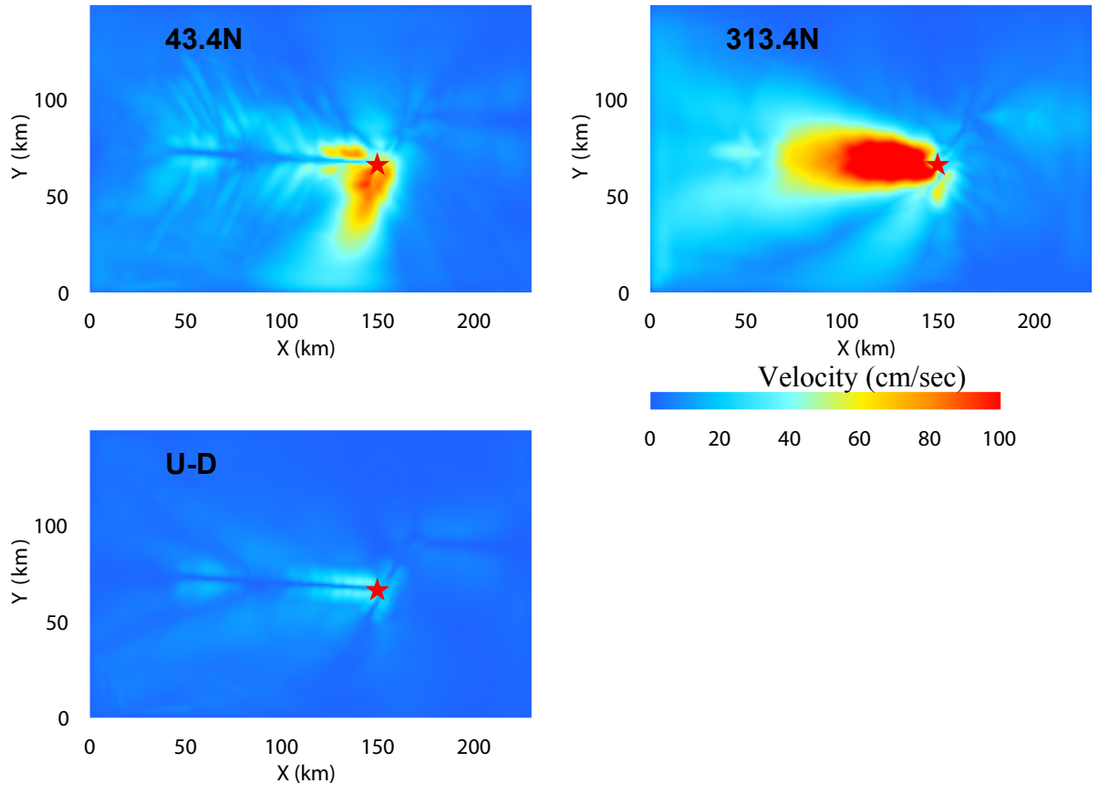

Figure 15. Peak velocity distribution obtained with the slip model with deep asperity and the hypocenter located on the west side of the fault. Star shows the epicenter locations.

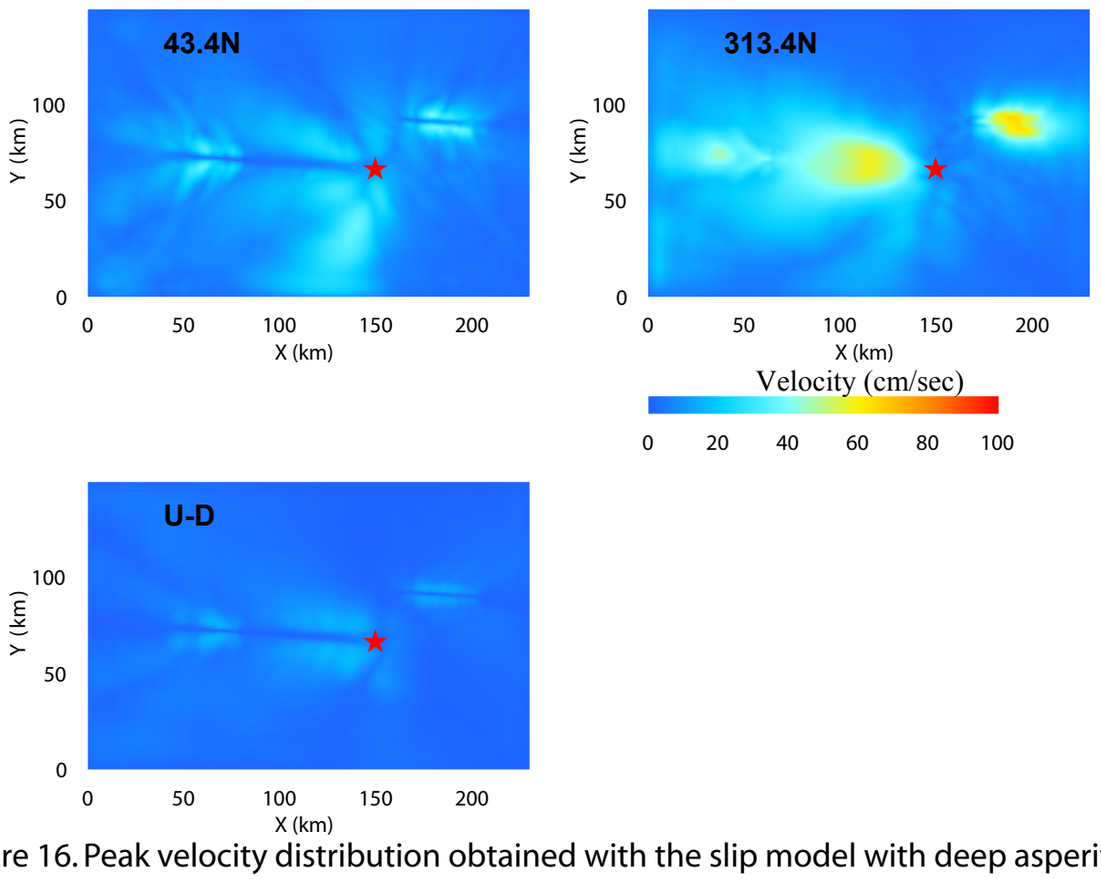

Figure 16. Peak velocity distribution obtained with the slip model with deep asperity, and the hypocenter located on the east side of the fault. Star shows the epicenter locations.

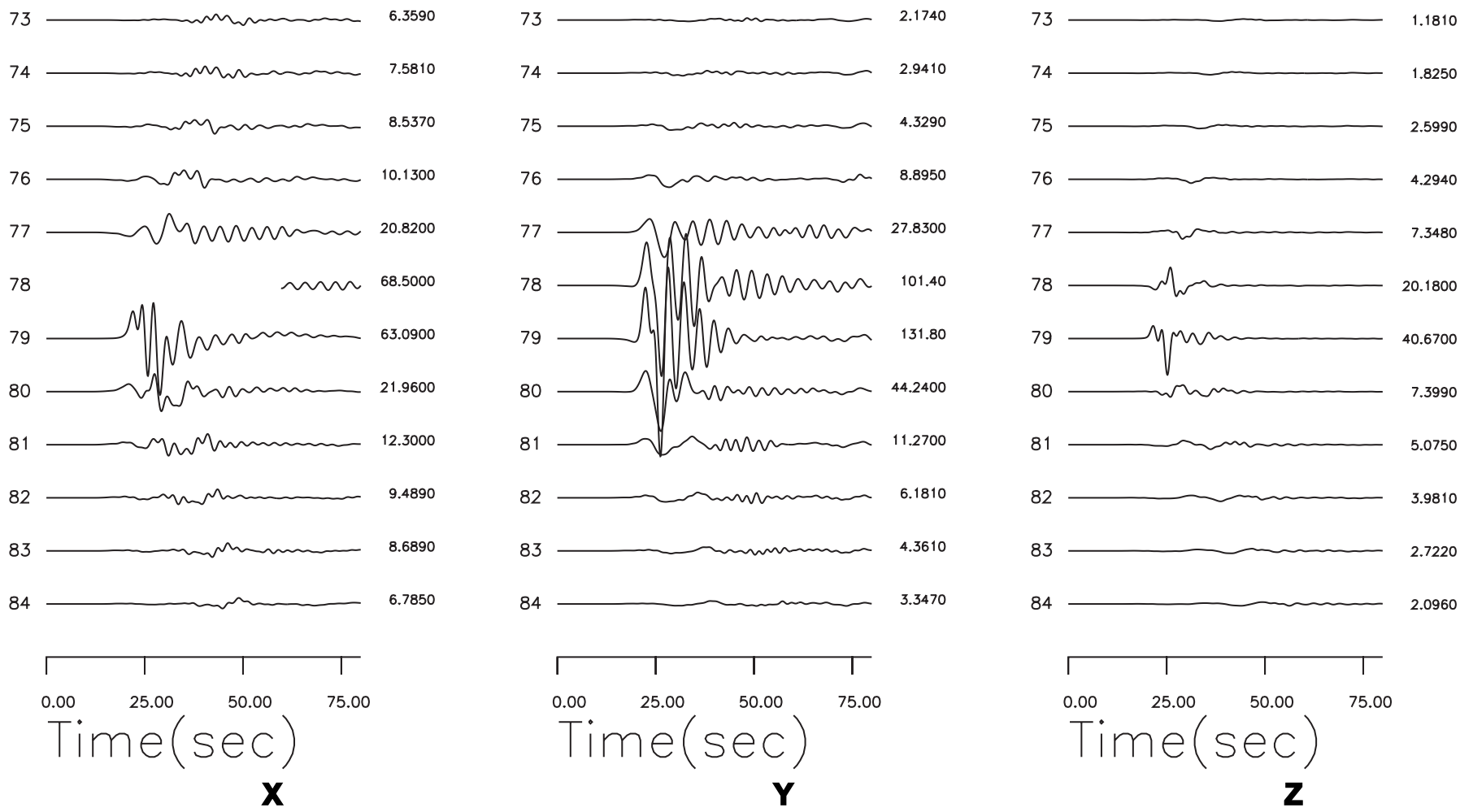

Figure 17. Synthetic section of finite-difference seismograms generated using the slip model with shallow asperity for the hypocenter located in the west. The section is shown for receivers along the line 73-84 across the basin as shown in Figure 10.

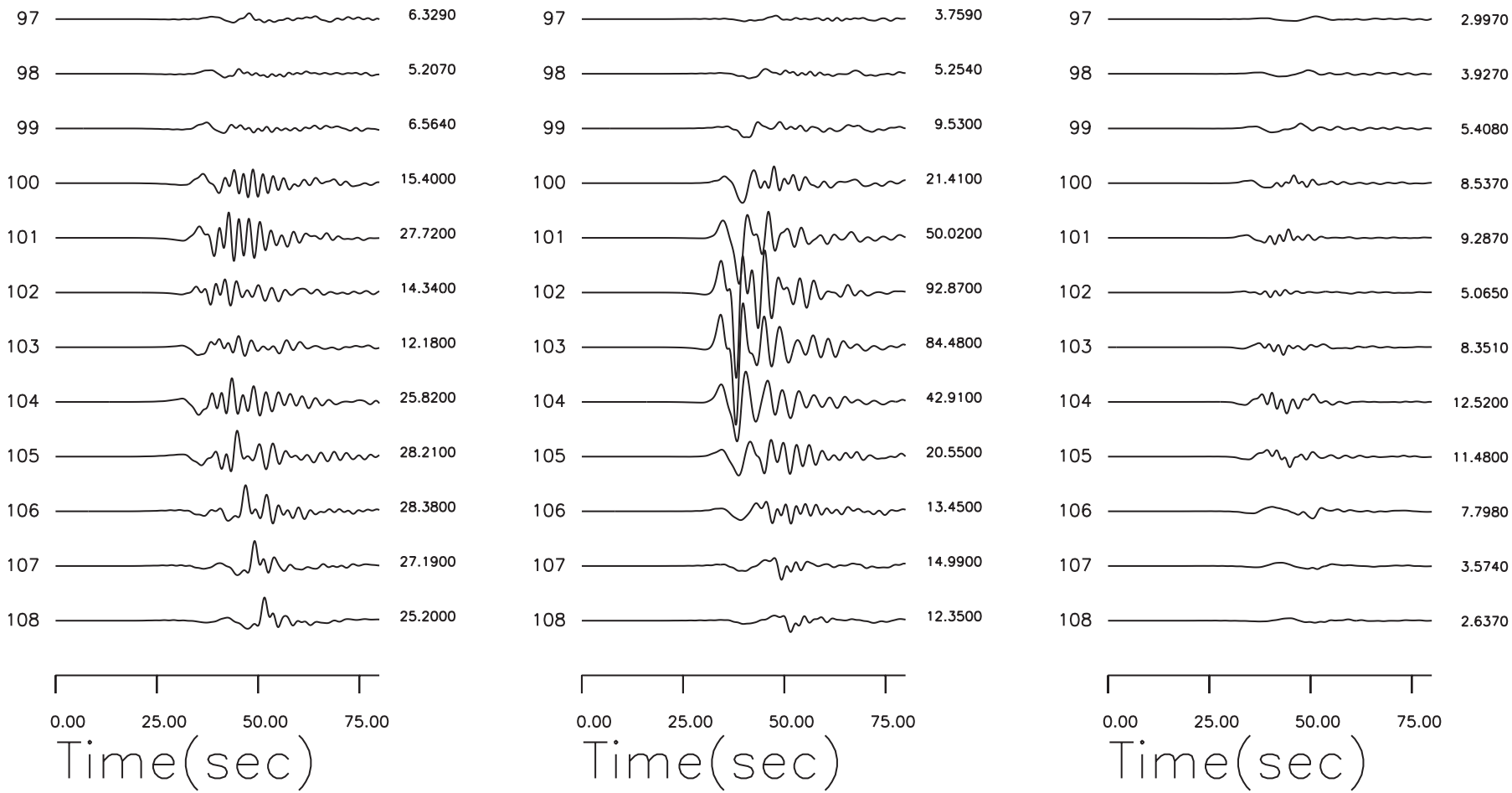

Figure 18. Caption for this figure is same as in Figure 17. The section is shown for receivers along the line 97-108 across the basin as shown in Figure 10.

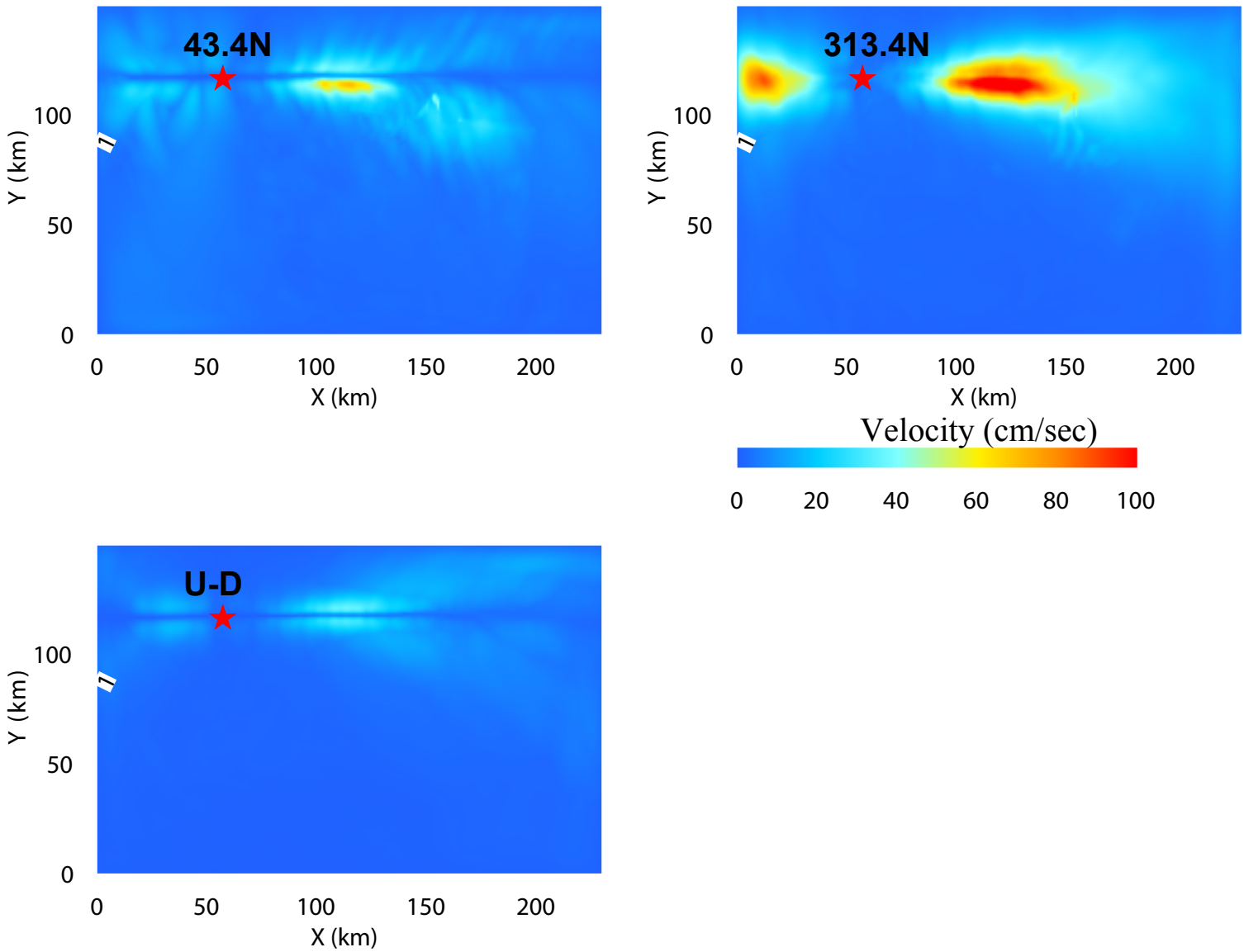

Figure 19. Peak velocity distribution simulated for the fifth scenario earthquake. The fault projection on the free surface is indicated by the green segment. Contour lines indicate the bedrock depth.

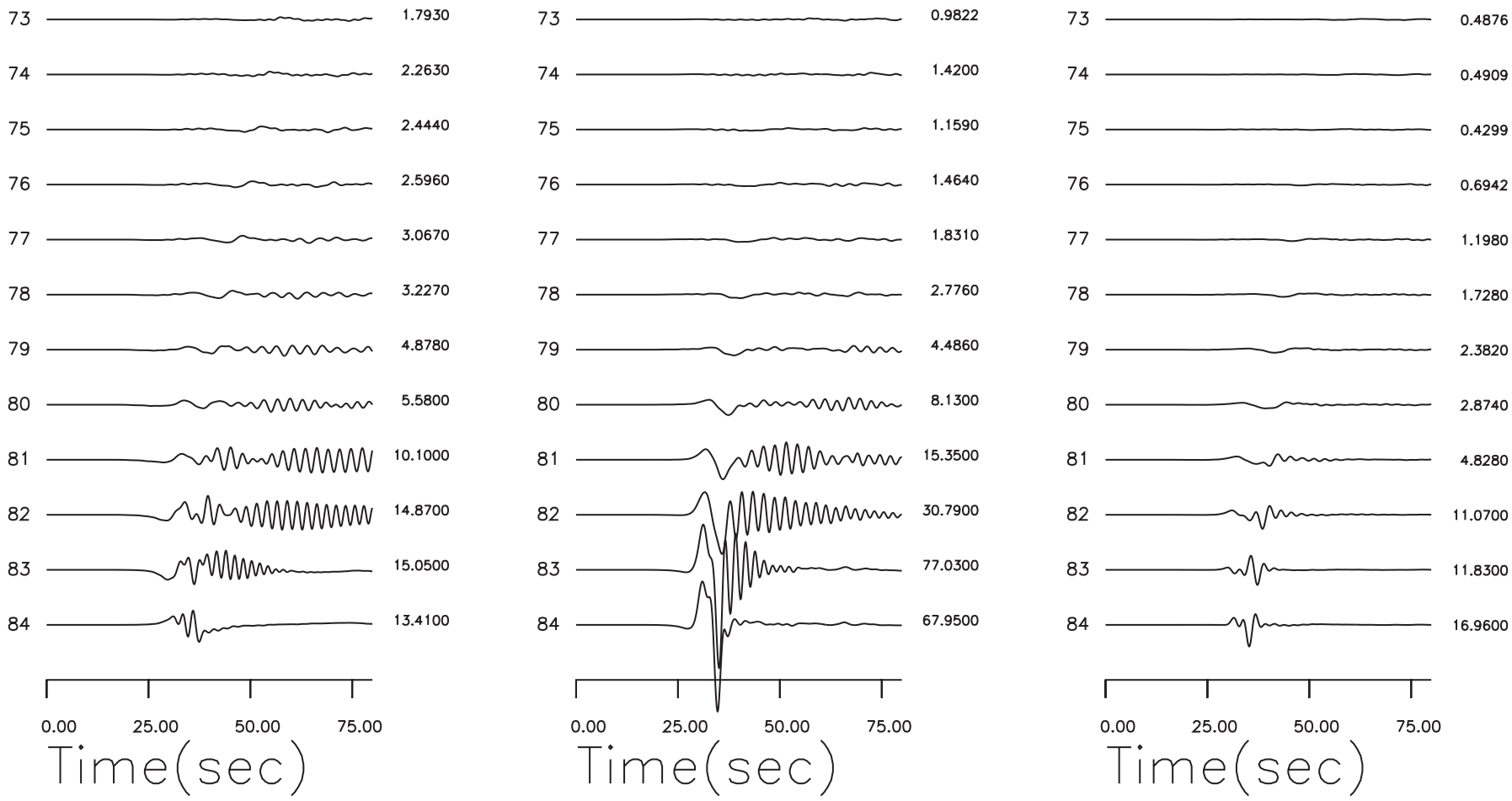

Figure 20. Synthetic seismic section generated for the fifth scenario earthquake fo0r a sigle fault instead of the multiple segments fault. The section is calculated along the line 73-84 across the basin as shown in Figure 10

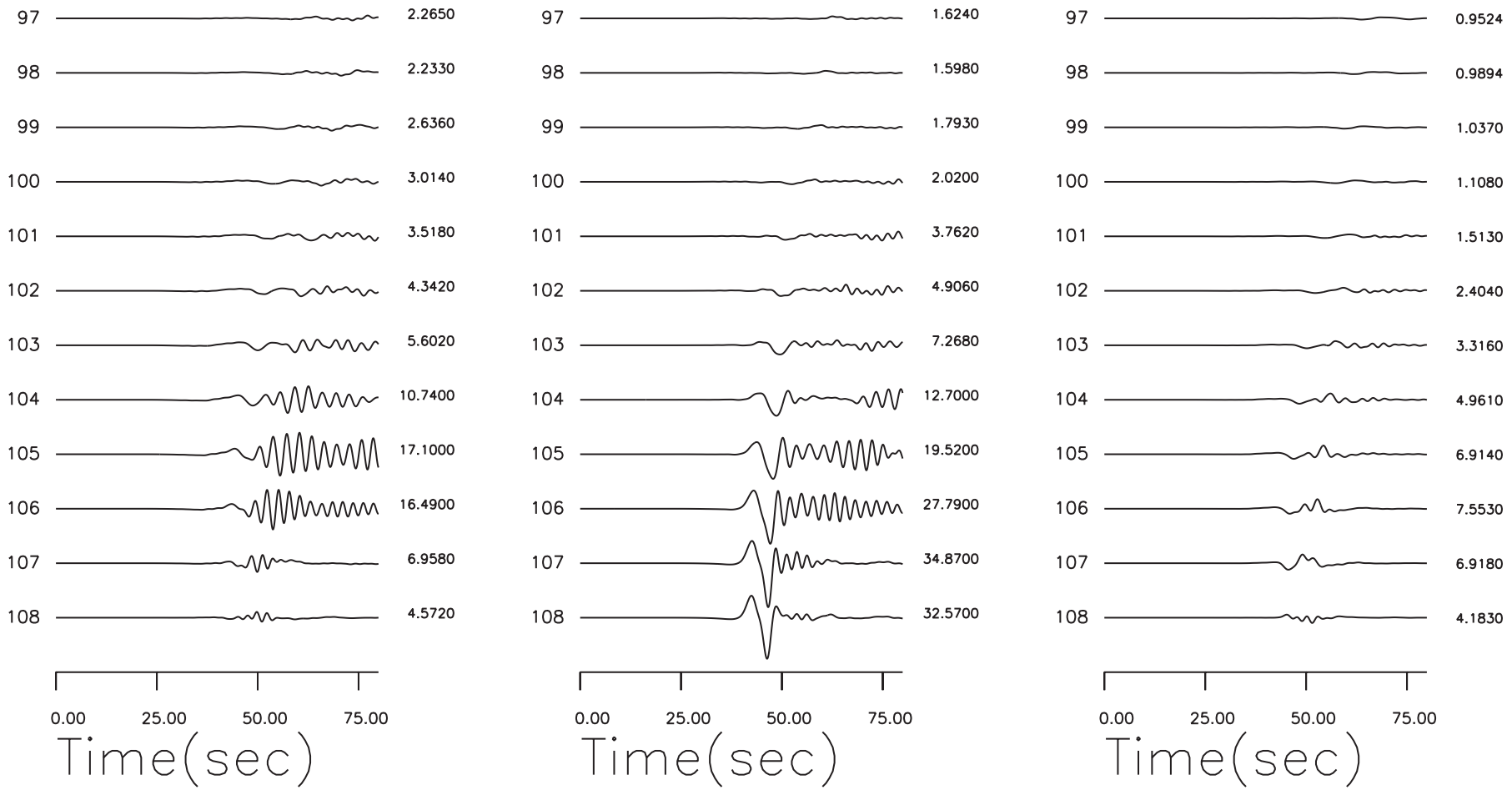

Figure 21. Caption for this figure is same as of Figure 20. The section is for receivers along the line 97-108 across the basin as shown in Figure 10.